

Fully Actuated Manifold Constraint Based Output Feedback Control for Input-Constrained Uncertain Nonlinear Systems

Dianrui Mu, Changchun Hua, Yafeng Li, Jiannan Chen, and Rao Wei *

May 21, 2026

Abstract

This paper presents a low-complexity, model-free, output-feedback controller for a class of unknown time-varying nonlinear systems with unknown input constraints. The controller achieves the preset control accuracy when the actuator is not saturated and maintains flexible control accuracy after actuator saturation. This result extends existing constraint control methods for linear manifolds to a more general form, including the construction of nonlinear manifolds and various types of constraints, thereby achieving preset control accuracy within finite or fixed time. Additionally, flexible control under unknown saturation is achieved through the construction of an error-driven flexible constraint. Finally, second-order and higher-order control examples and simulations are provided.

Keywords: Fully actuated manifold constraint, output feedback, prescribed performance, uncertain nonlinear systems.

1 Introduction

1.1 Motivation

Based on observations of different control methods below, control modeling and state acquisition, handling uncertainties, feedback form and performance guarantee are almost the most basic three issues of system control.

1.1.1 Control modeling and state acquisition

Control system modeling is a prerequisite for analyzing and designing. There are three modeling methods according to the state selection and the differential equation form. *Model1*: First-order state space

equations [1] is a common modeling approach according to the physical system mechanisms. Nonlinear and uncertain terms are dispersed into first-order differential equations one by one, so they need to be addressed one by one. The acquisition of these physical states depends on sensors or state observers. Based on universal approximator, the output feedback problem of uncertain nonlinear systems can be solved in [2] and [3], however, with a complex structure. The output feedback design without approximator usually has various limitations on the system: unit gain coefficient [4], known control gain [5], known nonlinear growth form [6], known nonlinear boundary form [7], etc. *Model2*: Under certain conditions [8], strict feedback systems can be transformed into high-order fully actuated systems concerning output through differential homeomorphism in high-order fully actuated system approaches (HFASA) [9]. The system is transformed into a standard form, and all gain coefficients and unmatched dynamics are combined into total gain and total disturbance, allowing for unified processing. Combining differentiators, output feedback can be achieved [10], but it needs the control gain bounds to be known. *Model3*: Furthermore, considering the tracking control problem, establishing a fully actuated error system model can further simplify the acquisition of the states, the derivative informations of the reference signal are no longer required in [11].

1.1.2 Handling uncertainties

Dealing with internal and external uncertainties in the system to ensure its stability and controllability is a basic requirement of the controller. The common methods to handle uncertainty are as follows. *Handle1*: Robust control including Bang-bang control, Parameter robust, Sliding mode control (SMC) [12], etc. It forces the error to converge by multiplying the upper bound of the uncertainty by the sign of the variable, but this also leads to controller chattering. *Handle2*: Adaptive control including Param-

*Authors Dianrui Mu, Changchun Hua, Yafeng Li, Jiannan Chen, and Rao Wei are with the Institute of Electrical Engineering, Yanshan University, Qinhuangdao, 066004, China (e-mail: mdr@stumail.yzu.edu.cn; cch@ysu.edu.cn; y.f.li@foxmail.com; cjn@ysu.edu.cn).

eter adaptive [13], Neural adaptive [3], Fuzzy adaptive [2], etc. The adaptive law can only estimate constant values. Although the adaptive method combining neural networks and fuzzy systems has universal approximation ability, its structure will become very complex. *Handle3*: Disturbance estimation including Extended state observer (ESO) [14], Disturbance observer (DO), Time delay control (TDC), etc. Although the ESO can estimate the total disturbance, it needs to use the total gain value (at least a rough estimate) [14]. *Handle4*: Dynamic gain including Low-complexity prescribed performance control (PPC) [15], etc. It can offset the impact of uncertainty by adjusting gains dynamically. Its structure is simple, but there is incompatibility between multiple constraints when dealing with high-order systems [16].

1.1.3 Feedback form and performance guarantee

The feedback form can directly determine the results of the Lyapunov stability analysis, thereby determining the performance of the system. Overall, the feedback form is a function of the states (or estimated states) and time. According to whether feedback variables are aggregated during use, feedback forms can be divided into two categories. *Form1*: Gradual feedback form is used in Backstepping, Cascade PID, etc. *Form2*: Aggregated feedback form is used in SMC, HFASA, etc. To improve performance, two fast feedback forms have been developed. *Fast1*: The power function feedback form is the function of the states, including finite-time control [17–19], fixed-time control [20–22], predefined time control [23], etc. *Fast2*: The time constrained feedback form is the function that depends on the states and time, including funnel control [24], PPC [25], low-complexity PPC [15], prescribed time control [26–28], etc.

The combination of gradual feedback, aggregated feedback, and fast feedback can form various feedback forms, such as fixed time sliding mode [29], prescribed time sliding mode [30], prescribed performance HFASA [31], etc. In recent years, a control method combining aggregated feedback and low-complexity PPC has been studied in [11,32–36]. Due to the manifolds used in them are all linear manifolds satisfying Hurwitz, we refer to it as linear manifold constraint control (LMCC). Among them, output feedback control is achieved in [32] and [11], while adaptive and integral control are combined in fault-tolerant PID (AFPID) control in [35] and [36]. The performance of these methods requires complex formulas to be expressed so that the steady-state accu-

racy cannot be preset directly.

1.2 Contributions

By integrating *Model3*, *Handle4*, *Form2*, and fast feedback form, a novel control method, fully actuated manifold constraint control (FAMCC), is proposed. The major contributions are summarized below:

- 1) The linear manifold constraint control method [11,32–36] is extended to nonlinear manifold constraint. It has the following characteristics:
 - **Model-free**: The designed controller does not use any model information, particularly, the final output feedback controller relies solely on the system’s output error.
 - **Prescribed performance**: The steady-state accuracy can be directly preset in the controller, and the convergence time can be given, which can not be achieved in LMCC [11,32–36].
 - **Flexibility and robustness**: An error-driven flexible constraint is proposed to achieve flexible control under input constraints. Compared to saturation-driven flexible constraints [37,38], the proposed method does not require any knowledge on the input constraints.
 - **Low complexity**: The controller design employs a low-complexity control method, which can ultimately be simplified into a very simple form.
- 2) For second-order systems, the ability of the proposed FAMCC under different combination schemes to converge to preset steady-state accuracy within finite time and fixed time is presented. Moreover, the discontinuity problem [39] in the variable exponent coefficient fixed-time control method [39–41] is solved.
- 3) For high-order systems, the fixed time convergence ability of the FAMCC based on the nonlinear manifold is proved through recursive analysis. It is shown that LMCC [11,32–34] are special cases of the proposed FAMCC with linear manifold.

2 Problem Formulation

2.1 Notation

For notation convenience, \mathcal{R} , \mathcal{R}^+ , \mathcal{R}^n , and $\mathcal{R}^{m \times n}$ denote the real space, the nonnegative real space,

the real n -dimensional space, and the real $m \times n$ -dimensional space, respectively. $\|\bullet\|$ is the Euclidean vector norm. $[z]^p = |z|^p \text{sign}(z)$. The arguments of the functions will be omitted or simplified whenever no confusion can arise from the context, e.g., $z(t)$ can be denoted by z .

2.2 Smooth transition function

It is often necessary to construct smooth functions when designing controllers to facilitate differential analysis and ensure that the controller is smooth or continuous. According to diverse needs, we introduce the following definitions:

Definition 1 Single-ended smooth transition function $\mathcal{T}(z)$ has the following properties:

- a $\mathcal{T}(z) = 0, \forall z \leq 0$, and $\mathcal{T}(1) = 1$;
- b The n -th order derivative of $\mathcal{T}(z)$ is continuous on $(-\infty, 1]$ and $\dot{\mathcal{T}}(z) \geq 0$.

Definition 2 Double-ended smooth transition function $\mathcal{S}(z)$ has the following properties:

- a $\mathcal{S}(z) = 0, \forall z \leq 0$, and $\mathcal{S}(z) = 1, \forall z \geq 1$;
- b The n -th order derivative of $\mathcal{S}(z)$ is continuous on \mathcal{R} and $\dot{\mathcal{S}}(z) \geq 0$.

Definition 3 Interval smooth transition function $\mathcal{U}(z)$ has the following properties:

- a $\mathcal{U}(0) = 0$, and $\mathcal{U}(z) = 1, \forall |z| \geq 1$;
- b The n -th order derivative of $\mathcal{U}(z)$ is continuous on \mathcal{R} ;
- c $\dot{\mathcal{U}}(z) \leq 0, \forall z \leq 0$ and $\dot{\mathcal{U}}(z) \geq 0, \forall z \geq 0$.

Remark 1 According to the definition, there are many selection forms for the smooth transition function mentioned above. Below is a set of examples:

$$\mathcal{T}(z) = \begin{cases} 0, & z \leq 0 \\ e^{\frac{z-1}{z}}, & 0 < z < 1 \end{cases} \quad (1)$$

$$\mathcal{S}(z) = \begin{cases} 0, & z \leq 0 \\ \frac{1}{e^{\frac{1-2z}{z(1-z)}} + 1}, & 0 < z < 1 \\ 1, & z \geq 1 \end{cases} \quad (2)$$

$$\mathcal{U}(z) = \mathcal{S}(|z|). \quad (3)$$

Any order derivatives of these functions are continuous.

Based on single-ended smooth transition function, a prescribed performance function can be defined as

$$\rho(\rho_0, \epsilon, T_\rho) = (\rho_0 - \epsilon)\mathcal{T}\left(\frac{T_\rho - t}{T_\rho}\right) + \epsilon \quad (4)$$

where $\rho_0 > \epsilon > 0$ and $T_\rho > 0$ are all positive constants. ρ_0 , ϵ , and T_ρ are the constraint on the initial state, prescribed accuracy, and settling time respectively.

2.3 System

The following strict-feedback uncertain nonlinear system is investigated in this article:

$$\begin{cases} \dot{x}_{oi} = g_i(\bar{x}_{oi}, t)x_{o(i+1)} + f_i(\bar{x}_{oi}, t) \\ \dot{x}_{on} = g_n(\bar{x}_{on}, t)u(v) + f_n(\bar{x}_{on}, t) \\ y_o = x_{o1} \end{cases} \quad (5)$$

where $i = 1, 2, \dots, n-1$ and $\bar{x}_{oi} = [x_{o1}, \dots, x_{oi}]^T \in \mathcal{R}^i$. $\bar{x}_{on} = [x_{o1}, \dots, x_{on}]^T \in \mathcal{R}^n$, $y_o \in \mathcal{R}$, $v \in \mathcal{R}$, and $u \in \mathcal{R}$ are the state vector, the system output, the to-be-designed controller, and actual control input provided by the actuator, respectively. The gain coefficients $g_i(\bar{x}_{oi}, t) \in \mathcal{R}^i \times \mathcal{R}^+ \rightarrow \mathcal{R}$ and unmatched dynamics $f_i(\bar{x}_{oi}, t) \in \mathcal{R}^i \times \mathcal{R}^+ \rightarrow \mathcal{R}$ are unknown time-varying nonlinear functions that locally Lipschitz in their arguments.

Assumption 1 $u(v) = v$ for all time.

Assumption 2 The i th-order ($1 \leq i \leq n-1$) derivatives of the reference signal y_d can be obtained.

Assumption 3 [11, 32, 33] The i th-order ($1 \leq i \leq n-1$) derivatives of the system output y_o are available.

Assumption 4 The reference signal y_d is a continuously differentiable and bounded function of time with bounded derivatives up to order n .

Assumption 5 The initial states of system $x_{oi}(0)$ with $1 \leq i \leq n$ are bounded.

Assumption 6 For $1 \leq i \leq n$, g_i , f_i and those $(n-i)$ th-order derivatives are continuous and bounded for $\|\bar{x}_{oi}\| \in L_\infty$. There exists an unknown positive constant \underline{G} such that $\prod_{i=1}^n g_i > \underline{G}$.

Assumption 7 There are unknown time-varying input constraints $\underline{u}(t) < 0 < \bar{u}(t)$ on $u(v)$, defined as:

$$u(v) = \begin{cases} \underline{u}, & v < \underline{u} \\ v, & \underline{u} \leq v \leq \bar{u} \\ \bar{u}, & v > \bar{u}. \end{cases} \quad (6)$$

Under these constraints, the system remains input-to-state stable (ISS) [37] or input-to-state practically stable (ISpS) [42].

Remark 2 Considering the various possibilities of the inherent characteristics of the system, the reference signal, and the initial states, not all input constraints can ensure the system remains stable. This is particularly true for self-excited divergent systems, such as $\dot{x} = x + u(v)$ with $\bar{u} = -\underline{u} = 1$, where if the reference signal or initial state leads to $|x| > 1$, no controller can drive the system back to stability. Therefore, in general, it is assumed that the system under input constraints remains ISS or ISpS.

Objective: For the system (5), under different assumptions as Table 1, the control objective is to design controllers such that the tracking error $z_1 = y_o - y_d$ converges to prescribed accuracy ϵ_z within finite/fixed time whenever actuation limitations allow, or flexible prescribed accuracy when the input constraints are reached.

3 Algorithm Architecture

The design framework of this method includes four parts/steps:

Step A. Fully actuated error system transformation.

Step B. Fully actuated manifold design.

Step C. Manifold constraint control.

Step D. Manifold constraint control under input constraints.

Step E. Differentiator-based manifold constraint control.

3.1 Fully Actuated Error System Transformation

Step A1: Fully actuated system transformation

After the differential homeomorphism transformation in the HFASA [9], the system (5) is transformed as follows:

$$\begin{cases} \dot{x}_i = x_{i+1}, & i = 1, 2, \dots, n-1 \\ \dot{x}_n = G_a(\bar{x}_{on}, t)u + F_a(\bar{x}_{on}, t) \\ y = x_1 \end{cases} \quad (7)$$

where total gain is $G_a = G_n$ and total disturbance is $F_a = F_n$ with $G_1 = g_1$, $F_1 = f_1$, $G_i = \prod_{k=1}^i g_k$, and $F_i = \dot{F}_{i-1} + \dot{G}_{i-1}x_{oi} + G_{i-1}f_i$ when $i = 2, \dots, n$.

Step A2: Fully actuated error system transformation

Define system errors as:

$$z_i = x_i - y_d^{(i-1)}, \quad i = 1, 2, \dots, n \quad (8)$$

The fully actuated errors system of (7) is

$$\begin{cases} \dot{z}_i = z_{i+1}, & i = 1, 2, \dots, n-1 \\ \dot{z}_n = Gu + F \end{cases} \quad (9)$$

where $G = G_a$ and $F = F_a - y_d^n$.

Define system the fully actuated state errors vector as:

$$\mathbf{Z}(t) = [z_1(t), \dots, z_n(t)]^T \in \mathcal{R}^n. \quad (10)$$

3.2 Fully Actuated Manifold Design

A manifold constructed by using all fully actuated errors is named fully actuated manifold.

Step B1: Iterative manifold design

To construct a linear/nonlinear manifold with a general form for n th-order systems, negative feedback functions $h_{mi}(\bullet)$, where $i = 1, \dots, n-1$, with the following properties, are introduced:

1. $h_{mi}(0) = 0$ and $\frac{\partial h_{mi}(\bullet)}{\partial \bullet} < 0, \forall 1 \leq i \leq n-1$.
2. $h_{m(n-1)}(\bullet)$ is continuous and differentiable, and its derivative $\frac{\partial h_{m(n-1)}(\bullet)}{\partial \bullet} \in L_\infty$ for $\bullet \in L_\infty \cap \Omega_0^c$ with $\Omega_0^c := \{\bullet \mid |\bullet| > 0\}$.
3. When $n > 2$ and $i = 1, \dots, n-2$, $h_{mi}(\bullet)$ and its $(n-i)$ th-order derivatives are continuous and bounded for bounded \bullet .

h_v is the inverse function of $h_{m(n-1)}$, which will be used later.

Referring to existing fast manifold design methods [43–45], the fully actuated manifold of an n -order system can be constructed using iterative methods as follows

$$\begin{cases} s_1 = z_1 \\ s_i = \dot{s}_{i-1} - h_{m(i-1)}(s_{i-1}), & i = 2, \dots, n \\ s = s_n \end{cases} \quad (11)$$

It is equivalent to

$$s = z_n - \sum_{i=1}^{n-1} h_{mi}^{(n-1-i)}(s_i). \quad (12)$$

Remark 3 A general representation of the fully actuated manifold is a mapping $h_g \in \mathcal{R}^n \rightarrow \mathcal{R}$, formed as $s = h_g(\mathbf{Z})$, which ensures that \mathbf{Z} tends towards $\mathbf{0}$ when $s = 0$. Referring to common manifold/filtered

Table 1: Control Objective.

Type	Feedback	Assumptions	Objective
O1	state feedback	Assumptions 1-6	prescribed accuracy
O2	state feedback	Assumptions 2-7	flexible prescribed accuracy
O3	output feedback	Assumptions 4-7	flexible prescribed accuracy

variable designs [11, 32–36], a linear fully actuated manifold is designed as $s = \sum_{i=1}^n a_i z_i$, where a_i are chosen such that the polynomial $\sum_{i=1}^n a_i \partial^{i-1}$ is Hurwitz with ∂ as Laplacian operator.

Step B2: Skewed manifold design

First of all, introduce a positive exponent coefficients feedback curve as follows:

$$S_p(s_i) := \{(s_i, \dot{s}_i) | \dot{s}_i - h_{pi}(s_i) = 0\} \quad (13)$$

where $h_{pi}(\bullet)$ is a function composed of one or more positive exponent coefficients feedback functions.

It is worth noting that simply constraining the fully actuated errors \mathbf{Z} near the linear manifold as [11, 32–36] cannot directly preset steady-state accuracy by a control parameter. It also can not obtain the finite/fixed time convergence to the preset accuracy results by just replacing the linear manifold with a corresponding finite/fixed time manifold [44, 45].

Therefore, the following provides two skewed manifold designs to construct h_{mi} based on positive exponent coefficients feedback h_{pi} .

3.2.1 Smooth Skewed Manifold Design (SSMD)

$$h_{mi}(s_i) = h_{pi}(s_i) + T_{1i}\epsilon_{si} \quad (14)$$

3.2.2 Nonsingular Skewed Manifold Design (NSMD)

$$h_{mi}(s_i) = T_{2i}(h_{pi}(s_i) + T_{1i}\epsilon_{si}) - (1 - T_{2i})k_{pi}s_i \quad (15)$$

where ϵ_{si} and ϵ_{zi} are positive constants which will be determined in specific use. $T_{1i} = 1 - 2\mathcal{S}\left(\frac{s_i + \epsilon_{zi}}{2\epsilon_{zi}}\right)$ is function constructed from double-ended smooth transition function defined in (2). $T_{2i} = \mathcal{U}\left(\frac{s_i}{\epsilon_{zi}}\right)$ is function constructed from interval smooth transition function defined in (3). $k_{pi} = k_{ppi} \frac{\epsilon_{si} - h_{pi}(\epsilon_{zi})}{\epsilon_{zi}}$ with positive constant k_{ppi} that can adjust the slope of the h_{mi} at $s_i = 0$.

Remark 4 Notably, as shown in Fig. 1, if $\frac{\partial h_{pi}}{\partial s_i}$ is singular at $s_i = 0$ with $\frac{\partial h_{pi}}{\partial s_i}(0) = -\infty$, SSMD can not

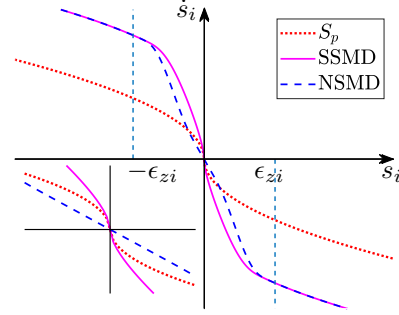


Figure 1: Skewed manifold design diagram.

change singularity, while NSMD can eliminate this singularity since T_{2i} and its arbitrary order derivatives are 0 at $s_i = 0$. This guarantees that, when employing a nonlinear negative feedback function in conjunction with the iterative method (11) to construct nonlinear manifolds of order higher than two, singularities will not occur for all derivatives of $\mathcal{U}(z)$ at $z = 0$ vanish.

3.3 Manifold Constraint Control

The state with a manifold variable of 0 is defined as zero manifold state

$$\mathbf{S}_0 := \{\mathbf{Z} | s = 0\}. \quad (16)$$

Step C1: Define the boundaries of manifold constraint regions:

Define the manifold translation function $s_m(x_m, y_m)$ as:

$$s_m(x_m, y_m) = \dot{s}_{n-1} - h_{m(n-1)}(s_{n-1} - x_m) - y_m \quad (17)$$

The upper boundary \mathbf{S}_U and lower boundary \mathbf{S}_L of the manifold constraint region are obtained by translating \mathbf{S}_0 as:

$$\mathbf{S}_U := \{\mathbf{Z} | s_m(x_U(t), y_U(t)) = 0\} \quad (18)$$

$$\mathbf{S}_L := \{\mathbf{Z} | s_m(x_L(t), y_L(t)) = 0\} \quad (19)$$

in which $x_L(t)$, $x_U(t)$, $y_L(t)$, and $y_U(t)$ are time-varying boundary offsets that satisfy $x_L \leq 0 \leq x_U$, $y_L \leq 0 \leq y_U$, and $x_L y_U = x_U y_L$.

The manifold constraint region is:

$$\Psi_s := \{\mathbf{Z} | s_m(x_L, y_L) > 0, s_m(x_U, y_U) < 0\}. \quad (20)$$

To ensure that the initial state of the system is within the manifold constraint region Ψ_s and establish constraints on performance, the boundary offsets should make the manifold constraint region large enough at the initial time, and the region Ψ_s continues to shrink over time, and eventually reach its minimum at preset time T_s and stop shrinking. Therefore, the prescribed performance function (4) is the ideal form of $-x_L(t)$, $x_U(t)$, $-y_L(t)$, and $y_U(t)$, e.g., as follows:

$$x_U = -x_L = \rho(k_0 \rho_{x0}, \epsilon_x, T_s) \quad (21)$$

$$y_U = -y_L = \rho(k_0 \rho_{y0}, \epsilon_y, T_s) \quad (22)$$

in which $\rho_{x0} = \max\{|s_{x0}|, \epsilon_x\}$ with s_{x0} being the initial value of $|h_v(\dot{s}_{n-1}) - s_{n-1}|$, and $\rho_{y0} = \max\{|s_{y0}|, \epsilon_y\}$ with s_{y0} being the initial value of $|h_m(n-1)(s_{n-1}) - \dot{s}_{n-1}|$. ϵ_x and ϵ_y are the final values of the lateral and vertical offset of the boundary, which can determine the size of the final constraint region Ψ_s . $k_0 > 1$ is a control coefficient that can adjust the initial control input since it can adjust the distance between the boundary $\mathbf{S}_L, \mathbf{S}_U$ and the initial state $(s_{n-1}(0), \dot{s}_{n-1}(0))$.

Manifold constraint can be divided into three types according to the direction of the boundary movement:

3.3.1 Oblique Manifold Constraint (OMC)

The boundary formed by \mathbf{S}_0 oblique displacement: $x_L y_U = x_U y_L \neq 0$ as in equation (21) and (22).

3.3.2 Longitudinal Manifold Constraint (LoMC)

The boundary formed by \mathbf{S}_0 vertical displacement: $x_L = x_U = 0, y_L y_U \neq 0$ as in equation (22).

3.3.3 Lateral Manifold Constraint (LaMC)

The boundary formed by \mathbf{S}_0 horizontal displacement: $y_L = y_U = 0, x_L x_U \neq 0$ as in equation (21).

Remark 5 For linear manifolds, the constraint boundaries obtained by using different translation methods are equivalent. Unlike linear manifolds, the constraint regions obtained by different translation

methods are different for nonlinear manifolds. Although no examples of adapting to OMC are found in this paper, this case is presented as the most general form of manifold constraints for future reference.

Remark 6 Unlike common prescribed performance functions that choose a fixed value or $+\infty$ as the initial value ρ_0 , this article uses multiples of the initial state values to construct the initial value of the performance function. This ensures that the initial state satisfies the constraints, while the initial value of the controller can be adjusted according to the coefficients k_0 .

Step C2: Calculate manifold constraint variables:

In this step, a manifold constraint variable ξ will be defined which can be used to represent the deviation of the state from the zero manifold state \mathbf{S}_0 within the manifold constraint region Ψ_s .

The projection of zero manifold state \mathbf{S}_0 , upper bound of the manifold constraint \mathbf{S}_U , and lower bound of the manifold constraint \mathbf{S}_L on the two-dimensional phase plane (s_{n-1}, \dot{s}_{n-1}) are as follows:

$$S_0 := \{(x, y) | y = h_m(n-1)(x)\} \quad (23)$$

$$S_U := \{(x, y) | y = h_m(n-1)(x - x_U) + y_U\} \quad (24)$$

$$S_L := \{(x, y) | y = h_m(n-1)(x - x_L) + y_L\} \quad (25)$$

Define gradient lines as

$$S_G := \left\{ (x, y) \left| \begin{cases} x_U y = y_U(x - s_{n-1}) + x_U \dot{s}_{n-1}, & \text{OMC} \\ x = s_{n-1}, & \text{LoMC} \\ y = \dot{s}_{n-1}, & \text{LaMC} \end{cases} \right. \right\} \quad (26)$$

The intersection point between the gradient line S_G and the manifold curve S_0 is (x_c, y_c) , which can be obtained by solving the following equation

$$x_U (h_m(n-1)(x_c) - \dot{s}_{n-1}) = y_U (x_c - s_{n-1}) \quad (27)$$

in OMC.

Define the manifold constraint variable $\xi(\mathbf{Z})$ as

$$\xi(\mathbf{Z}) = \begin{cases} 2 \frac{s_{n-1} - x_c - x_L}{x_U - x_L} - 1, & \text{OMC} \\ 2 \frac{s - y_L}{y_U - y_L} - 1, & \text{LoMC} \\ 2 \frac{s_{n-1} - h_v(\dot{s}_{n-1}) - x_L}{x_U - x_L} - 1, & \text{LaMC} \end{cases} \quad (28)$$

When the state approaches the lower boundary S_L , ξ tends towards -1 , and when the state approaches the upper boundary S_U , ξ tends towards 1 . Therefore, as long as the manifold constraint variable ξ is

constrained within $(-1, 1)$, the s can be constrained within the constraint region Ψ_s .

Step C3: Design manifold constraint controller:

A manifold constraint controller is designed as follows:

$$v(\mathbf{Z}) = -k_u \Gamma(\xi(\mathbf{Z})) \quad (29)$$

where k_u is positive constant. $\Gamma(\bullet)$ is a monotonic odd function mapped from interval $(-1, 1)$ to interval $(-\infty, \infty)$, e.g., $\frac{\xi}{(1+\xi)(1-\xi)}$ and $\ln(\frac{1+\xi}{1-\xi})$.

3.4 Manifold Constraint Control Under Input Constraints

Taking into account the unknown input constraints, the error-driven flexible boundaries of the manifold constraints are designed as

$$\begin{aligned} \tilde{x}_U = -\tilde{x}_L &= (1 - \mathcal{T}_s)x_U + \mathcal{T}_s \frac{d_{sc} + \rho_e}{d_U} x_U \\ \tilde{y}_U = -\tilde{y}_L &= (1 - \mathcal{T}_s)y_U + \mathcal{T}_s \frac{d_{sc} + \rho_e}{d_U} y_U \end{aligned} \quad (30)$$

where $\mathcal{T}_s = \mathcal{S}\left(\frac{d_{sc} - (d_U - \rho_e)}{\rho_e}\right)$, $d_U = \sqrt{x_U^2 + y_U^2}$, and $d_{sc} = \sqrt{(s_{n-1} - x_c)^2 + (\dot{s}_{n-1} - y_c)^2}$ with $\rho_e \ll \sqrt{\epsilon_x^2 + \epsilon_y^2}$ being a small positive constant.

The associated flexible constraint variable is defined as

$$\tilde{\xi}(\mathbf{Z}) = \begin{cases} 2 \frac{s_{n-1} - x_c - \tilde{x}_L}{\tilde{x}_U - \tilde{x}_L} - 1, & \text{OMC} \\ 2 \frac{s - \tilde{y}_L}{\tilde{y}_U - \tilde{y}_L} - 1, & \text{LoMC} \\ 2 \frac{s_{n-1} - h_v(\dot{s}_{n-1}) - \tilde{x}_L}{\tilde{x}_U - \tilde{x}_L} - 1, & \text{LaMC} \end{cases} \quad (31)$$

and the corresponding flexible manifold constraint controller is designed as

$$v(\mathbf{Z}) = -k_u \Gamma(\tilde{\xi}(\mathbf{Z})). \quad (32)$$

3.5 Differentiator-based Manifold Constraint Control

The system (9) can be rewritten as

$$\begin{cases} \dot{\mathbf{Z}} = \mathcal{A}\mathbf{Z} + \mathcal{B}(Gu + F) \\ z_1 = \mathcal{C}\mathbf{Z} \end{cases} \quad (33)$$

where $\mathcal{A} = \begin{bmatrix} \mathbf{0}_{n-1} & \mathbf{I}_{n-1} \\ 0 & \mathbf{0}_{n-1}^T \end{bmatrix}$, $\mathcal{B} = [\mathbf{0}_{n-1}^T \quad 1]^T$, $\mathcal{C} = [1 \quad \mathbf{0}_{n-1}^T]$ in which $\mathbf{I}_{n-1} \in \mathcal{R}^{(n-1) \times (n-1)}$ and $\mathbf{0}_{n-1} \in$

\mathcal{R}^{n-1} are identity matrix and zero column vector, respectively.

A high gain differentiator used to obtain an estimate $\hat{\mathbf{Z}}$ of the actual fully actuated errors \mathbf{Z} is designed as

$$\begin{cases} \dot{\hat{\mathbf{Z}}} = \mathcal{A}\hat{\mathbf{Z}} + H_\mu(z_1 - \mathcal{C}\hat{\mathbf{Z}}) \\ \hat{z}_1(0) = z_1(0) \end{cases} \quad (34)$$

with $H_\mu = \text{diag}(\frac{a_1}{\mu}, \frac{a_2}{\mu^2}, \dots, \frac{a_n}{\mu^n})$ where μ is a sufficiently small positive constant and $a_i (i = 1, \dots, n)$ are chosen such that the polynomial $\partial^n + \sum_{i=1}^n a_i \partial^{n-i}$ is Hurwitz.

Replacing all the actual fully actuated errors \mathbf{Z} in the controller (32) with the estimate $\hat{\mathbf{Z}}$, the output feedback controller is designed as

$$v(\hat{\mathbf{Z}}) = -k_u \Gamma(\tilde{\xi}(\hat{\mathbf{Z}})) \quad (35)$$

4 Fully Actuated Manifold Constraint Theorem

Similar to SMC, FAMCC has two stages: approaching the zero manifold S_0 before T_s and moving along the vicinity of the zero manifold S_0 after T_s .

In this section, it is only proven that the controller has the ability to drive and constrain the system full drive error \mathbf{Z} to the vicinity of the zero manifold S_0 , that is, the stage of approaching the manifold. The final ability to converge the output error z_1 to the preset accuracy ϵ_z in a finite/fixed time, i.e., the stage of moving along the vicinity of the manifold, will be demonstrated in subsequent corollaries.

4.1 Lemma

Lemma 1 *Considering the manifold design in (11) and the manifold constraint variable $\xi(\mathbf{Z})$ in (28) for the system (5) under Assumptions 4-6, if $|\xi(\mathbf{Z})| < 1, \forall t \geq 0$, then it holds that all $s_i(t)$ and $z_i(t), i = 1, \dots, n$ remain bounded.*

Proof: See Appendix A. ■

4.2 State Feedback

Theorem 1 *For the system (5), under Assumptions 1-6, if the controller (29) is applied, then it holds that:*

- (i) all closed-loop signals are bounded for all $t \geq 0$;
- (ii) $\mathbf{Z}(t) \in \Psi_s$ in (20), and $|\xi(\mathbf{Z})| < 1$ for all $t \geq 0$;
- (iii) there exist positive constants \tilde{u} such that $|u| \leq \tilde{u}, \forall t \geq 0$.

Proof: See Appendix B. ■

4.3 State Feedback Under Input Constraints

Theorem 2 For the system (5), under Assumptions 2-7, if the controller (32) is applied with sufficiently small ρ_e , then it holds that:

- (i) When the actuator output capability is sufficient, the conclusion is same as the Theorem 1 (i) and (ii);
- (ii) When the actuator output capability is insufficient, it can be ensured that the fully actuated errors $\mathbf{Z}(t)$ remains within a flexible constraint set $\tilde{\Psi}_s$

$$\tilde{\Psi}_s := \{s_m(\tilde{x}_L, \tilde{y}_L) > 0, s_m(\tilde{x}_U, \tilde{y}_U) < 0\}. \quad (36)$$

The flexible constraint boundaries (30) will be flexibly expanded after the controller (32) reaches input constraints (6), ensuring the controller (32) is well-defined and the closed-loop system continues to operate effectively. Furthermore, the constraint boundaries are fully restored to their original values (i.e., $\tilde{x}_U = -\tilde{x}_L = x_U = -x_L$ and $\tilde{y}_U = -\tilde{y}_L = y_U = -y_L$) when the controller exits saturation.

Proof: See Appendix C. ■

Remark 7 It is worth noting that the designed flexible controller has the following new features:

- a. The flexible constraint designed does not rely on input constraint information as [37, 38], enabling a more thorough model-free control approach;
- b. Unlike existing adaptive flexible boundaries [37, 38], which recover slowly and cannot return to the original constraints within finite time, the proposed flexible controller can immediately restore the original constraints once saturation ends.
- c. The required parameter ρ_e is sufficiently small and can be easily tuned for successful implementation. Even if the selected ρ_e is not sufficiently small, the controller will continue to increase until the input constraints are reached, thereby ensuring the full utilization of the actuator's output capacity.

4.4 Output Feedback Under Input Constraints

Theorem 3 For the system (5), under Assumptions 4-7, if the differentiator (34) and the controller (35) are applied, then there exists a constant $\bar{\mu} \in (0, 1)$ such that the conclusion is same as Theorem 2 when $0 < \mu < \bar{\mu}$.

Proof: See Appendix D. ■

Remark 8 The proof of the Theorem 3 can also refer to [32] and [11]. Since $z_1 = y_o - y_d$ is known, setting the initial value of the differentiator $\hat{z}_1(0)$ to be the same as $z_1(0)$ in (34) can make the estimated value converge faster.

4.5 Corollaries

According to the Theorem 1, Theorem 2, and Theorem 3, the controller (29), (32), and (35) only implements constraints on the manifold, i.e., \mathbf{Z} always stays within Ψ_s . The performance of the system output is related to the constructed manifold, the selected manifold constraint type, and their parameters. The controller design provided in the section 3, including two skewed types (SSMD / NSMD) and three manifold constraint types (OMC / LoMC / LaMC), can form many controller combinations by combining different feedback functions.

For ease of understanding, we will first demonstrate the controller's ability to converge to preset accuracy $z_1 < \epsilon_z$ in finite and fixed time for second-order systems in sections 5. Further, the fixed time convergence ability of the controller for high-order systems is demonstrated in sections 6.2. The corresponding corollaries will be provided and proven. The configuration used for the control of each section is shown in the TABLE 2 below.

Remark 9 It is worth noting that a very direct idea is to directly impose a constraint on manifold s . This is equivalent to LoMC without skewed design, as explained in the subsequent simplification of (50). However, it is difficult to preset control accuracy through control parameters by only s -constraint. Existing research [32] and [35] has provided the relationship between accuracy and control parameters such that it must reverse deduce control parameters according to accuracy requirements when using only s -constraint. Furthermore, fast sliding mode (nonlinear manifold), such as [29] and [40], is a mature method to achieve faster convergence speed. However, it is even more difficult to provide the relationship between performance and control parameters in only s -constraint, so skewed manifold design methods in Step B2 and manifold constraint methods in Step C1 are designed specially in this article. By combining the fast manifold and LaMC, it is easy to preset accuracy and provide the convergence time as shown in section 5.1. However, considering that solving the inverse function of complex functions can be very complex, this approach is only suitable for simple fast manifolds. To

Table 2: Composition of controllers in section 5.

Section	Feedback function	Constraint types	Skewed types
5 Second-order Systems			
5.1	Finite-time	LaMC	none
5.2	Variable exponent coefficients fixed-time	LoMC	SSMD
6 High-order Systems			
6.1	Linear fully actuated manifold	OMC/LoMC /LaMC	none
6.2	Iterative fixed-time fully actuated manifold	LoMC	NSMD

achieve faster convergence, more complex fast manifolds are often required, which is the starting point of designing skewed manifolds in this article. Many fast manifolds (or SMC), such as [29] and [40], can preset accuracy and provide the setting time by combining with skewed design, that will be presented in the example given in section 5.2 and 6.2.

5 Second-order Systems Control

To present our design ideas more clearly, the case of system (5) with $n = 2$ (a second-order system) is considered at the first. The positive exponent coefficients feedback has many forms that conform to the definition of negative feedback function, such as function with low exponent coefficients in finite-time control [18], function composed of low and high exponent coefficients function in fixed-time feedback [29] and variable exponent coefficients feedback [40].

5.1 LaMC Based Finite-time PPC

Finite-time feedback law is selected as negative feedback function h_{m1} :

$$h_{m1}(s_1) = -k_c [s_1]^p, 0 < p < 1 \quad (37)$$

Under LaMC, the controller (35) can be simplified as follows:

$$\begin{aligned} v &= -k_u \ln \left(\frac{1 + \xi}{1 - \xi} \right) \\ &= -k_u \ln \left(\frac{1 + \left(2 \frac{s_{n-1} - h_v(\dot{s}_{n-1}) - \tilde{x}_L}{\tilde{x}_U - \tilde{x}_L} - 1 \right)}{1 - \left(2 \frac{s_{n-1} - h_v(\dot{s}_{n-1}) - \tilde{x}_L}{\tilde{x}_U - \tilde{x}_L} - 1 \right)} \right) \quad (38) \\ &= -k_u \ln \left(\frac{s_{n-1} - h_v(\dot{s}_{n-1}) - \tilde{x}_L}{\tilde{x}_U - s_{n-1} + h_v(\dot{s}_{n-1})} \right) \end{aligned}$$

It can be observed that $s_{n-1} - h_v(\dot{s}_{n-1}) = s_{n-1} + \frac{1}{k_c} [\dot{s}_{n-1}]^{\frac{1}{p}}$ is a common form of nonsingular finite-time sliding surface. Defined it as

$$s_{fn} = s_{n-1} + \frac{1}{k_c} [\dot{s}_{n-1}]^{\frac{1}{p}}, 0 < p < 1 \quad (39)$$

The controller (38) can be further simplified as

$$v = -k_u \ln \left(\frac{s_{fn} - \tilde{x}_L}{\tilde{x}_U - s_{fn}} \right), \quad (40)$$

while \tilde{x}_L and \tilde{x}_U can be simplified as

$$\begin{aligned} \tilde{x}_U &= -\tilde{x}_L \\ &= (1 - \mathcal{T}_x)x_U + \mathcal{T}_x(|h_v(\dot{s}_{n-1}) - s_{n-1}| + \rho_e) \quad (41) \\ &= (1 - \mathcal{T}_x)x_U + \mathcal{T}_x(|s_{fn}| + \rho_e) \end{aligned}$$

with $\mathcal{T}_x = \mathcal{S} \left(\frac{|s_{fn}| - (x_U - \rho_e)}{\rho_e} \right)$.

This indicates that the LoMC on finite-time manifolds with (37) is equivalent to a constraint on nonsingular finite-time manifold value s_{fn} in (39).

Corollary 1 For the system (5) with $n = 2$ under Assumptions 4-7, if the high gain differentiator (34) and the controller (40) (which is equivalent to (35) composed of (11), (21), (28), and (37)) is used with parameter selection $\epsilon_x = \epsilon_z$ in (21) and sufficiently small ρ_e, μ , the close-loop system has the following properties:

- (i) When the actuator output capability is sufficient, the setting time T_{fn} for z_1 to converge to the accuracy $|z_1| < \epsilon_z$ satisfies the following inequality:

$$T_{fn} < T_s + T'_{fn} \quad (42)$$

with $T'_{fn} = \frac{z_1^{1-p}(0)}{k_c(1-p)}$;

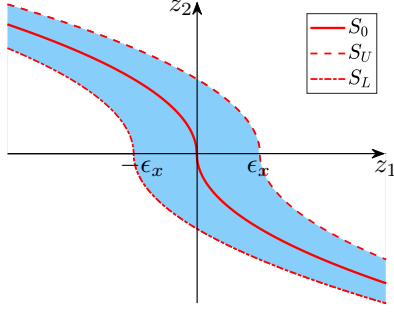


Figure 2: LaMC based finite-time manifold constraint diagram after T_s .

(ii) When the actuator output capability is insufficient, the system achieves a flexible control accuracy $|z_1| < \tilde{x}_U$ within the same finite time T_{fn} , and after the controller exits saturation, it recovers to the preset accuracy ϵ_z within a finite time $(\max\{T_e, T_s\} + T'_{fn})$ where T_e is the time when the system exits saturation.

Proof: According to **Theorem 3**, if the controller is used with $u = v, \forall t \geq 0$, \mathbf{Z} always stays within Ψ_s , i.e., \mathbf{Z} will stay within the blue area in the Fig. 2 after T_s . Therefore, the following inequality holds:

$$\begin{cases} z_2 > k_c |z_1 + \epsilon_x|^p, & z_1 < -\epsilon_x \\ z_2 < -k_c |z_1 - \epsilon_x|^p, & z_1 > \epsilon_x \end{cases} \quad (43)$$

Referring to the finite time control theorem [18], z_1 will converge to $z_1 > -\epsilon_x$ in finite time for $z_1(0) < 0$ and converge to $z_1 < \epsilon_x$ in finite time for $z_1(0) > 0$. The convergence time T_{fn} is expressed as (42), which is related to T_s , the initial state and the parameters of h_{m1} in (37). The final accuracy is determined by ϵ_x which can be set as ϵ_z .

When the controller becomes saturated and the manifold constraint boundary is expanded, the system state will enter the flexible constraint set $\tilde{\Psi}_s$ (36) as the design in (30). Similar to the above analysis, the flexible accuracy is \tilde{x}_U . After exiting saturation, if the exit time T_e is earlier than the preset time T_s , the time to converge to the preset accuracy ϵ_z remains T_{fn} . If the exit time is later than the preset time $T_e \geq T_s$, the time to restore the preset accuracy will not exceed $(T_e + T'_{fn})$. ■

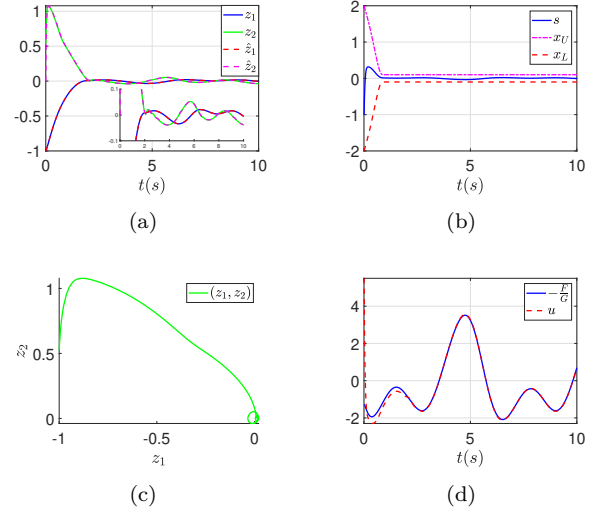


Figure 3: Simulation results of the finite-time PPC with LaMC. (a) The variables z_1 , z_2 , \hat{z}_1 , and \hat{z}_2 versus time. (b) The variables s_{fn} , x_U , and x_L versus time. (c) Phase trajectory (z_1, z_2) . (d) The evolution of $-\frac{F}{G}$ and u .

The following system is used in the simulation:

$$\begin{cases} \dot{x}_1 = (1 + 0.1 \cos(x_1) + 0.1 \sin(t))x_2 - x_1 + \sin(t) \\ \dot{x}_2 = (2 + 0.2 \sin(x_1 x_2) + 0.1 \cos(t))u(v) \\ \quad - (x_1^2 - 1)x_2 + \sin(t) + \cos(2t) \\ y = x_1, \underline{u} = -100, \bar{u} = 100, \\ x_1(0) = -1, x_2(0) = 0.5, y_d(t) = \sin(t). \end{cases} \quad (44)$$

The controller parameters are selected as follows: $k_u = 5, k_0 = 2, \epsilon_x = 0.1, T_s = 1, \rho_e = 0.01$ in controller, $k_c = 1, p = 0.5$ in (37), and $a_1 = 4, a_2 = 4, \mu = 0.01$ in differentiator (34), therefore $T_{fn} < 3$.

The simulation results are shown in Fig. 3(a)-Fig. 3(d). It can be intuitively seen that s_{fn} always evolves within the prescribed bounds x_U and x_L , and z_1 achieves the prescribed accuracy of 0.1 within the settling time of $1.9s < T_{fn}$.

With the control parameters set as described above, the input constraint in the system (44) is reduced to $\underline{u} = -2.5, \bar{u} = 3$. The simulation results are shown in Fig 4. The actuator output u remains within the input constraint at all times as Fig. 4(d). The flexible constraint \tilde{x}_U, \tilde{x}_L expands as $|s|$ increases, and it restores to its original preset value after exiting saturation as Fig. 4(b). The control accuracy is also able to recover to the preset accuracy within a finite time as Fig. 4(a).

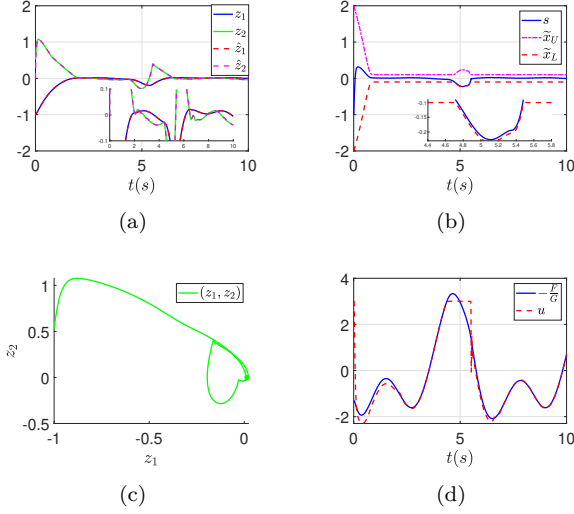


Figure 4: Simulation results of the finite-time PPC with LaMC and saturated actuator. (a) The variables z_1 , z_2 , \hat{z}_1 , and \hat{z}_2 versus time. (b) The variables s , \hat{x}_U , and \hat{x}_L versus time. (c) Phase trajectory (z_1, z_2) . (d) The evolution of $-\frac{F}{G}$ and u .

5.2 LoMC and SSMD Based Variable Exponent Coefficients Fixed-time PPC

A fixed time sliding surface with variable exponential coefficients is proposed in [40] and [41], but it is discontinuous [39]. An improved form is proposed below:

$$h_{p1}(s_1) = -k_c [s_1]^p \quad (45a)$$

$$p = \frac{as_1^2}{1 + bs_1^2} + r_b \quad (45b)$$

$$a = (r_t - r_b)b, b = \frac{r_1 - r_b}{r_t - r_1} \quad (45c)$$

$$z_2 = -k_c [z_1]^p + 2\epsilon_y \quad (46)$$

$$z_2 = -k_c [z_1]^p \quad (47)$$

$$z_2 = -k_c [z_1]^p - 2\epsilon_y \quad (48)$$

$$\begin{cases} p < 1, & 0 \leq |z_1| < 1 \\ p = 1, & |z_1| = 1 \\ p > 1, & |z_1| > 1 \end{cases} \quad (49)$$

where $0 < r_b < 1 < r_1 < r_t$. Select the negative feedback function h_{m1} based on SSMD (14) with (45).

Under LoMC, the controller (35) can be simplified

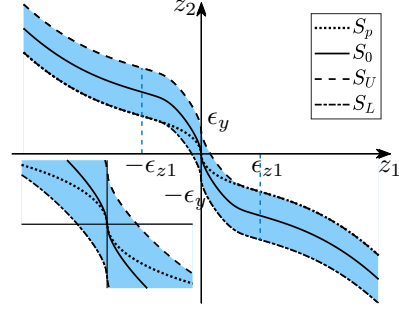


Figure 5: LoMC and SSMD based variable exponent coefficients fixed-time manifold constraint diagram after T_s .

as

$$\begin{aligned} v &= -k_u \ln \left(\frac{1 + \tilde{\xi}}{1 - \tilde{\xi}} \right) \\ &= -k_u \ln \left(\frac{1 + \left(2 \frac{s - \tilde{y}_L}{\tilde{y}_U - \tilde{y}_L} - 1 \right)}{1 - \left(2 \frac{s - \tilde{y}_L}{\tilde{y}_U - \tilde{y}_L} - 1 \right)} \right) \\ &= -k_u \ln \left(\frac{s - \tilde{y}_L}{\tilde{y}_U - s} \right) \end{aligned} \quad (50)$$

while \tilde{y}_L and \tilde{y}_U can be simplified as

$$\begin{aligned} \tilde{y}_U &= -\tilde{y}_L \\ &= (1 - \mathcal{T}_y)y_U + \mathcal{T}_y(|h_{m(n-1)}(s_{n-1}) - \dot{s}_{n-1}| + \rho_e) \\ &= (1 - \mathcal{T}_y)y_U + \mathcal{T}_y(|s| + \rho_e) \end{aligned} \quad (51)$$

where $\mathcal{T}_y = \mathcal{S} \left(\frac{|s| - (y_U - \rho_e)}{\rho_e} \right)$.

Corollary 2 For the system (5) with $n = 2$ under Assumptions 4-7, if the high gain differentiator (34) and the controller (50) (which is equivalent to (35) composed of (11), (14), (22), (28), and (45)) is used with parameters selection as

$$\begin{aligned} \epsilon_{s1} &= \epsilon_y \\ \epsilon_{z1} &= \epsilon_z \end{aligned} \quad (52)$$

in (22), (14) and sufficiently small ρ_e, μ , the close-loop system has the following properties:

- (i) When the actuator output capability is sufficient, the setting time T_{fxe} for z_1 to converge to the accuracy $|z_1| < \epsilon_z$ satisfies the following inequality:

$$T_{fxe} < T_s + T'_{fxe}. \quad (53)$$

$$\text{with } T'_{fxe} = \frac{1}{k_c(r_1 - 1)} + \frac{1}{k_c e^{-\frac{a}{2e}}(1 - r_b)};$$

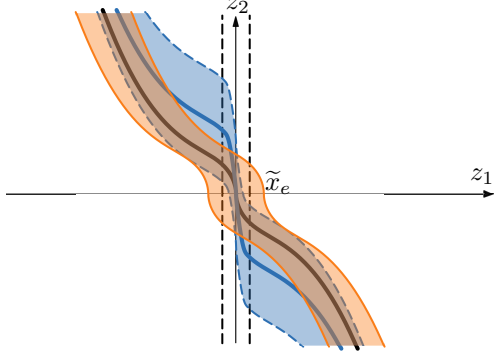


Figure 6: A schematic diagram of equivalent longitudinal flexible expansion achieved through lateral flexible expansion. The thick black curve represents $z_2 = h_{p1}(z_1)$, the black dashed line represents $z_1 = \pm\epsilon_{z1}$, and the thick blue solid line represents $z_2 = h_{m1}(z_1)$ with SSMD (14). The orange area is formed by the lateral expansion of $z_1 = \pm\epsilon_{z1}$, while the blue area is the result of the longitudinal elastic expansion of the manifold $z_2 = h_{m1}(z_1)$ into $\tilde{\psi}_s$.

- (ii) When the actuator output capability is insufficient, the system achieves a flexible control accuracy $|z_1| < \tilde{x}_e$ within the same fixed time T_{fxe} , and after the controller exits saturation, it recovers to the preset accuracy ϵ_z within a finite time $(\max\{T_e, T_s\} + T'_{fxe})$.

Proof: According to **Theorem 3**, if the controller is used with non-activated saturation, \mathbf{Z} always stays within Ψ_s , i.e., the blue area in the Fig. 5. The ϵ_{s1} in (14) is selected to be equal to the ϵ_y in (22). Then, S_L will overlap with S_p for $z_1 < -\epsilon_{z1}$, and S_U will overlap with S_p for $z_1 > \epsilon_{z1}$ after T_s as shown in Fig. 5. Therefore, the following inequality holds:

$$\begin{cases} z_2 > k_c |z_1|^p, & z_1 < -\epsilon_{z1} \\ z_2 < -k_c z_1^p, & z_1 > \epsilon_{z1} \end{cases} \quad (54)$$

The maximum time T_{max} required for a system $z_2 = \dot{z}_1 = -k_c [z_1]^p$ to converge to 0 is derived as below.

For $z_1 \geq 0$, it holds that

$$\begin{cases} z_2 \leq -k_c z_1^{r_1}, & z_1 \geq 1 \\ z_2 \leq -k_c z_1^{a z_1^{2+r_b}} \leq -k_c e^{-\frac{a}{2e}} z_1^{r_b}, & 0 \leq z_1 < 1 \end{cases} \quad (55)$$

where $\min\{z_1^{z_1^2}\} = e^{-\frac{1}{2e}}$. It leads to

$$z_1(t) \leq \begin{cases} (z_1^{1-r_1}(0) - k_c(1-r_1)t)^{\frac{1}{1-r_1}}, & t < t_1 \\ (z_1^{1-r_b}(t_1) - k_c(1-r_b)t)^{\frac{1}{1-r_b}}, & t_1 \leq t < t_2 \\ 0, & t \geq t_2 \end{cases} \quad (56)$$

where t_1 and t_2 are the first moment of $z_1(t) = 1$ and $z_1(0) = 0$, respectively. $t_1 \leq \frac{z_1^{1-r_1}(0)-1}{k_c(1-r_1)} = \frac{1}{k_c(r_1-1)}$, $t_2 \leq t_1 + \frac{z_1^{1-r_b}(t_1)}{k_c e^{-\frac{a}{2e}}(1-r_b)} = t_1 + \frac{1}{k_c e^{-\frac{a}{2e}}(1-r_b)}$. Therefore $T_{max} = \frac{1}{k_c(r_1-1)} + \frac{1}{k_c e^{-\frac{a}{2e}}(1-r_b)}$. The situation for $z_1 \leq 0$ is same as above.

By comparison, the system composed of inequality (54) has a faster convergence speed when $|z_1| > \epsilon_{z1}$, so the convergence time to $|z_1| \leq \epsilon_{z1}$ is less than T_{max} . The final accuracy is determined by ϵ_{z1} which can be set as ϵ_z .

When the controller becomes saturated and the system state will remain within the flexible constraint set $\tilde{\Psi}_s$ (36). Since $p \geq r_1 > 1$ for $|s_1| \geq 1$ in (45), there must exist a lateral flexible expansion set for non skewed manifolds (as shown in the orange area of Fig. 6)

$$\tilde{\Psi}_{se} := \{\mathbf{Z} | h_{p1}(z_1 + \tilde{x}_e) < z_2 < h_{p1}(z_1 - \tilde{x}_e)\} \quad (57)$$

which achieves slightly lower control accuracy \tilde{x}_e than the flexible constraint set $\tilde{\Psi}_s = \{\mathbf{Z} | h_{m1}(z_1) + \tilde{y}_L < z_2 < h_{m1}(z_1) + \tilde{y}_U\}$ formed for longitudinal flexible expansion of skewed manifolds (as shown in the blue area of Fig. 6) at a fixed time. The manifold $h_{m1}(z_1) + \tilde{y}_U$ and $h_{p1}(z_1 - \tilde{x}_e)$ intersect at only one point in the fourth quadrant. The curves $z_2 = h_{m1}(z_1) + \tilde{y}_U$ and $z_2 = h_{p1}(z_1 - \tilde{x}_e)$ intersect at only one point in the fourth quadrant. The shapes of the two curves, $\frac{\partial h_{p1}(0)}{\partial z_1} = -\infty$ and $-\infty < h_{m1}(z_1) < 0 \forall z_1 \neq 0$, ensure that there is always a solution that guaranteeing a unique intersection in the fourth quadrant as Fig. 6.

Similar to the previous analysis in proof of corollary 1, the flexible accuracy is \tilde{x}_e . After exiting saturation, if the exit time T_e is earlier than the preset time T_s , the time to converge to the preset accuracy ϵ_z remains T_{fxe} . If the exit time is later than the preset time $T_e \geq T_s$, the time to restore the preset accuracy will not exceed $(T_e + T'_{fxe})$. ■

Remark 10 The variable exponential coefficient function proposed in the [40] and [41] is

$$h_p(z) = -\beta [z]^p \quad (58a)$$

$$p(z) = \frac{\lambda_1 z^2}{1 + \mu_1 z^2}, \theta_1 = \frac{\lambda_1}{1 + \mu_1} > 1, \beta > 0 \quad (58b)$$

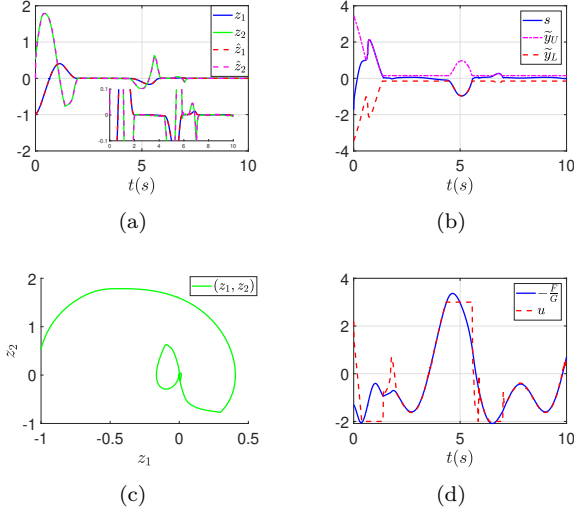


Figure 7: Simulation results of the fixed-time PPC with (45), LoMC, SSMD, and saturated actuator. (a) The variables z_1 , z_2 , \hat{z}_1 , and \hat{z}_2 versus time. (b) The variables s , \tilde{y}_U , and \tilde{y}_L versus time. (c) Phase trajectory (z_1, z_2) . (d) The evolution of $-\frac{F}{G}$ and u .

which has an exponential coefficient of 0 when $z = 0$, resulting in the value of $h_p(0)$ is -1 and the left limit is $\lim_{z \rightarrow 0^-} h_p(z) = 1$. Therefore, the sliding surface is discontinuous [39]. There is a jumping feedback form at the equilibrium point, with similar behavior as a sign term. In fact, if the exponential coefficient $p(z)$ is set as $p(z) = 0$, it is the sign function. Therefore, the controller's chattering can be seen in the simulation example of [40] and [41]. The design in (45) improves the variable exponential coefficient function by adjusting the exponential coefficients of the power feedback function at $z = 0$, $|z| = 1$, and $|z| = \infty$ using three parameters r_b , r_1 , and r_b , respectively, while ensuring that the lowest exponential coefficients r_b is greater than 0, thus guaranteeing the continuity of the function.

The simulation system is same as (44) with input constraint parameters $\underline{u} = -2$, $\bar{u} = 3$. The controller parameters are selected as follows: $k_u = 2$, $k_0 = 2$, $\epsilon_{s1} = \epsilon_y = 0.15$, $T_s = 1$, $\epsilon_{z1} = \epsilon_z = 0.1$, $k_{pp1} = 1$, $\rho_e = 0.01$ in controller, $k_c = 1.5$, $r_b = 0.5$, $r_1 = 2$, $r_t = 3$ in (45), and $a_1 = 4$, $a_2 = 4$, $\mu = 0.01$ in differentiator (34), therefore $T_{fxe} = 4.3$.

The simulation results are shown in Fig. 9. The actuator output u remains within the input constraint as Fig. 7(d). The flexible constraint \tilde{y}_U, \tilde{y}_L expands as s exceeds the original constraint y_U, y_L as Fig. 7(b), after exiting saturation, it restores to its original preset value y_U, y_L . The control accuracy is also

able to recover to the preset accuracy within a fixed time as Fig. 7(a).

6 High-order Systems Control

6.1 Linear Fully Actuated Manifold Constraint Control

Linear feedback law is selected as negative feedback function h_{mi} :

$$h_{mi}(s_i) = -b_i s_i \quad (59)$$

The manifold constructed based on iterative methods (11) is:

$$s = \prod_{i=1}^{n-1} \left(\frac{\partial}{\partial t} + b_i \right) s_1 \quad (60)$$

The polynomial (60) has $n - 1$ negative real poles $-b_i, i = 1, 2, \dots, n - 1$, which obviously satisfies the Hurwitz condition. It is consistent with the designs in many literature [11, 32–36]. The linear manifold is a straight line on the $(s_{n-1}, \dot{s}_n - 1)$ phase plane, so the effects of OMC, LaMC, and LoMC are the same. According to equation (50), the constraint on the linear manifold is ultimately a direct constraint on the value s . Therefore, LMCC [11, 32–34] are special cases of the proposed FAMCC with linear manifold.

6.2 FAMCC Based Recursive Fixed-time Control (RFC)

An iterative fixed-time fully actuated manifold can be constructed by (11), NSMD (15), LoMC (22), and fixed-time feedback law as follows:

$$h_{pi}(s_i) = -\alpha_i [s_i]^{p_i} - \beta_i [s_i]^{q_i}, i = 1, \dots, n - 1 \quad (61)$$

where p_i and q_i are positive constants which satisfy $0 < p_i < 1 < q_i$.

Corollary 3 For the system (5), under Assumptions 4-7, if the high gain differentiator (34) and the recursive fixed-time controller composed of (11), (15), (22), (61) and (35) (which also can be simplified as (50) under LoMC) is applied with parameters selection as:

$$\epsilon_{zj} = \epsilon_{s(j-1)}, \quad j = 2, \dots, n - 1 \quad (62a)$$

$$\epsilon_{z1} = \epsilon_z, \epsilon_{s(n-1)} = \epsilon_y \quad (62b)$$

in (22), (14) and sufficiently small ρ_e, μ , the close-loop system has the following properties:

- (i) When the actuator output capability is sufficient, the setting time T_{fr} for z_1 to converge

to the accuracy $|z_1| < \epsilon_z$ satisfies the following inequality:

$$T_{fr} < T_s + T'_{fr} \quad (63)$$

$$\text{with } T'_{fr} = \sum_{i=1}^{n-1} \left(\frac{1}{\alpha_i(1-p_i)} + \frac{1}{\beta_i(q_i-1)} \right);$$

(ii) When the actuator output capability is insufficient, the system achieves a flexible control accuracy $|s_j| < \tilde{x}_{ej}$ and $|z_1| < \tilde{x}_{e1}$

$$\begin{aligned} \tilde{x}_{e(n-1)} &= \max\{\epsilon_{z(n-1)}, \tilde{y}_U - y_U\}, \\ \tilde{x}_{ej} &= \max\{\epsilon_{zj}, \tilde{x}_{e(j+1)}\}. \end{aligned} \quad (64)$$

within the same fixed time T_{fr} , and after the controller exits saturation, it recovers to the preset accuracy ϵ_z within a finite time $\left(\max\{T_e, T_s\} + T'_{fr}\right)$ where T_e is the time when the system exits saturation.

Proof: Define manifold constrain region of (s_i, \dot{s}_i) with $i = 1, 2, \dots, n-1$ as follows:

$$\Psi_{si} := \{(s_i, \dot{s}_i) | -\epsilon_{si} < \dot{s}_i - h_{mi}(s_i) < \epsilon_{si}\} \quad (65)$$

where $\Psi_{s(n-1)} = \Psi_s$ in (20) after T_s since $\epsilon_{s(n-1)} = \epsilon_y$.

When the actuator output capability is sufficient, $u = v$ can be guaranteed during the operation. According to **Theorem 3**, if the controller is used with parameter selection (62), \mathbf{Z} always stays within Ψ_s , i.e., $|s| = |s_n| < \epsilon_{n-1} = \epsilon_y$ and (s_{n-1}, \dot{s}_{n-1}) always in $\Psi_{s(n-1)}$ after T_s . It can be obtained that the following inequality holds:

$$\begin{cases} \dot{s}_i > \alpha_i |s_i|^{p_i} + \beta_i |s_i|^{q_i}, & s_i < -\epsilon_{zi} \\ \dot{s}_i < -\alpha_i s_i^{p_i} - \beta_i s_i^{q_i}, & s_i > \epsilon_{zi} \end{cases} \quad (66)$$

for $i = n-1$. Referring to the fixed time control theorem [29], since s_{n-1} has faster converge speed than fixed-time system form (66), s_{n-1} will converge to $|s_{n-1}| < \epsilon_{z(n-1)} = \epsilon_{s(n-2)}$ within a fixed time $T_s + \frac{1}{\alpha_{n-1}(1-p_{n-1})} + \frac{1}{\beta_{n-1}(q_{n-1}-1)}$.

For $i = n-2, \dots, 1$, it can be recursively obtained that the inequality (66) holds when $|s_{i+1}| \leq \epsilon_{si}$. Combining the fixed time control theorem, s_i will converge to $|s_i| < \epsilon_{zi}$ within fixed time $T_s + \sum_{k=i}^{n-1} \left(\frac{1}{\alpha_k(1-p_k)} + \frac{1}{\beta_k(q_k-1)} \right)$. Recurring from $i = n-2$ to $i = 1$, it can be obtained that the final output accuracy is $|z_1| = |s_1| < \epsilon_{z1}$, and the convergence time T_{fr} can be expressed as (63), which is related to T_s and the parameters of h_{pi} in (61). The final accuracy is determined by ϵ_{z1} which can be set as ϵ_z .

When the actuator output capability is insufficient, the system state will remain within the flexible constraint set $\tilde{\Psi}_s$ (36) as the design in (30). For $i = 1, \dots, n-1$, since $\frac{\partial h_{pi}(s_i)}{\partial s_i} < -1, \forall s_i \in \mathcal{R}$ in (61), $\frac{\partial h_{mi}(s_i)}{\partial s_i} < -1, \forall |s_i| \geq \epsilon_{zi}$, the performance change caused by a lateral movement of a certain distance of h_{pi} is greater than the performance change caused by the same distance of longitudinal movement. Thus, the performance of the flexible constraint set $\tilde{\Psi}_s$, formed by the longitudinal flexible expansion of h_{mi} with NSMD (15), can be approximated by the constraint set $\tilde{\Psi}_{si}$, formed by the lateral flexible expansion of h_{pi} as

$$\tilde{\Psi}_{si} := \{(s_i, \dot{s}_i) | h_{pi}(s_i + \tilde{x}_{ei}) < \dot{s}_i < h_{pi}(s_i - \tilde{x}_{ei})\} \quad (67)$$

where \tilde{x}_{ei} is defined in (64). Similar to the previous analysis in proof of corollary 1, the flexible accuracy is denoted as $|s_i| \leq \tilde{x}_{ei}$. Recursively, the final flexible accuracy is obtained as \tilde{x}_{e1} .

After exiting saturation, if the exit time T_e is earlier than the preset time T_s , the time to converge to the preset accuracy ϵ_z remains T_{fr} . If the exit time is later than the preset time $T_e \geq T_s$, the time to restore the preset accuracy will not exceed $\left(T_e + T'_{fr}\right)$. ■

To verify the effectiveness of the proposed FAMCC based on RFC, the following system is used in the simulation:

$$\begin{cases} \dot{x}_1 = (1 + 0.1 \sin(x_1) + 0.1 \cos(t)) - x_1 + \cos(t), \\ \dot{x}_2 = (1 + 0.1 \cos(x_1 x_2) + 0.1 \sin(t)) x_3 \\ \quad - (x_1^2 - 1) x_2 + \sin(t), \\ \dot{x}_3 = (2 + 0.2 \sin(x_1 x_2 x_3) + 0.1 \cos(t)) u(v) \\ \quad - (x_1^2 + x_2) x_3 + 10 \sin(t) + 10 \cos(2t) \\ y = x_1, \underline{u} = -100, \bar{u} = 100, \\ x_1(0) = 1, x_2(0) = -0.2, x_3(0) = 0.4 \\ y_d(t) = \sin(t). \end{cases} \quad (68)$$

The controller parameters are selected as follows: $k_u = 30, k_0 = 2, \epsilon_{z1} = \epsilon_z = 0.1, \epsilon_{s1} = \epsilon_{z2} = 0.2, \epsilon_{s2} = \epsilon_y = 5, T_s = 1, k_{pp1} = 0.1, k_{pp2} = 1, \rho_e = 0.01$ in controller, $p_1 = p_2 = 0.5, q_1 = q_2 = 2, \alpha_1 = 1, \beta_1 = 0.5, \alpha_2 = 2, \beta_2 = 1$ in (61), and $a_1 = 4, a_2 = 6, a_3 = 4, \mu = 0.01$ in differentiator (34), therefore $T_{fx} < 7$.

The simulation results are shown in Fig. 8(a)-Fig. 8(f). It can be seen that s always evolves within the prescribed bounds y_U and y_L , and z_1 achieves the prescribed accuracy of 0.1 within the settling time of $1.2s < T_{fr}$.

If the input constraint in the system (68) is reduced to $\underline{u} = -7, \bar{u} = 9$. The simulation results are shown in Fig. 9. The actuator output u remains within the

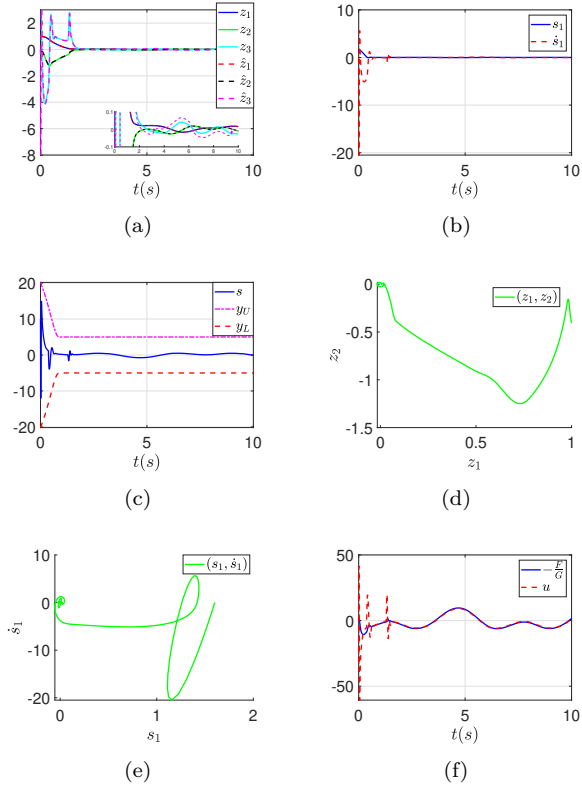


Figure 8: Simulation results of the RFC. (a) The variables z_1 , z_2 , z_3 , \hat{z}_1 , \hat{z}_2 and \hat{z}_3 versus time. (b) The variables s, \hat{s}_1 versus time (c) The variables s, y_U , and y_L versus time. (d) Phase trajectory (z_1, z_2) . (e) Phase trajectory (s_1, \hat{s}_1) . (f) The evolution of $-\frac{F}{G}$ and u .

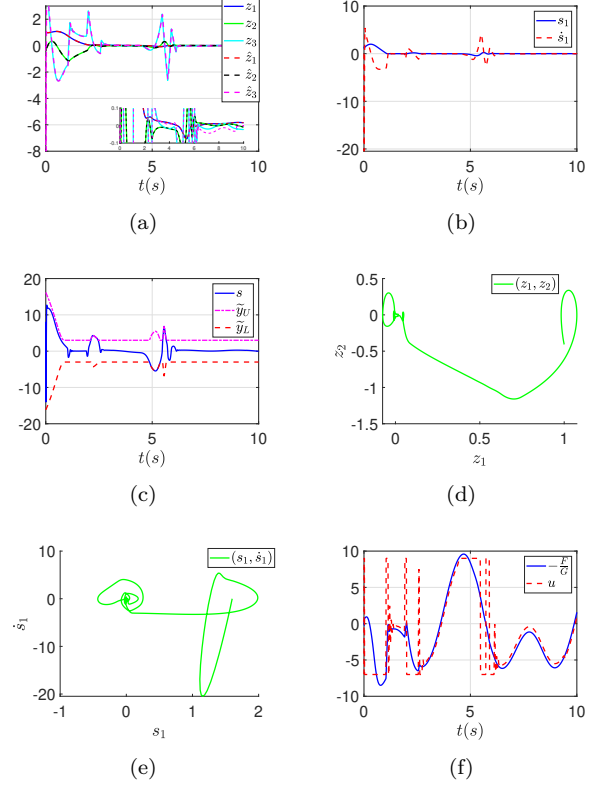


Figure 9: Simulation results of the RFC with saturated actuator. (a) The variables z_1 , z_2 , z_3 , \hat{z}_1 , \hat{z}_2 and \hat{z}_3 versus time. (b) The variables s, \hat{s}_1 versus time (c) The variables s, \tilde{y}_U , and \tilde{y}_L versus time. (d) Phase trajectory (z_1, z_2) . (e) Phase trajectory (s_1, \hat{s}_1) . (f) The evolution of $-\frac{F}{G}$ and u .

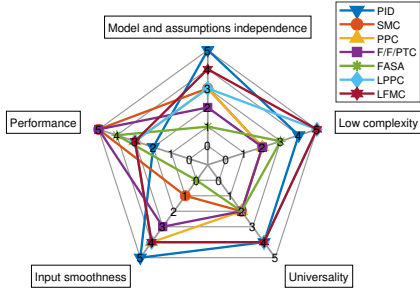


Figure 10: Comparison of characteristics of different controllers.

input constraint as Fig. 9(f). The flexible constraint \tilde{y}_U, \tilde{y}_L expands as s increases in Fig. 9(c), after exiting saturation, it restores to its original preset value y_U, y_L . The control accuracy is also able to recover to the preset accuracy within a fixed time as Fig. 8(a).

The MATLAB simulation codes can be obtained at <https://github.com/Mudianrui/FAMCC-SAT>.

7 Conclusion

7.1 Characteristics of This Methods

- (i) The linear manifold constraint control method [11, 32–36] is extended to nonlinear manifold constraint so that the steady-state accuracy can be directly preset in the controller.
- (ii) The final approximation-free controller only uses the output and the order of the system without various limitations on the system as [4–7] and [10].
- (iii) In the simulation, the controller almost coincides with the normalized total disturbance $-\frac{F}{G}$, demonstrating the ability to approximate the optimal energy.

7.2 Extension on This Methods

For the future researches, further improvements are required as follows:

- (i) Remove the assumption of model differentiability in Assumption 6. This may require the use of nonsmooth dynamic theory based on Filippov.
- (ii) The proposed control method exhibits low complexity characteristics in the control of a second-order system, but as the order increases, the

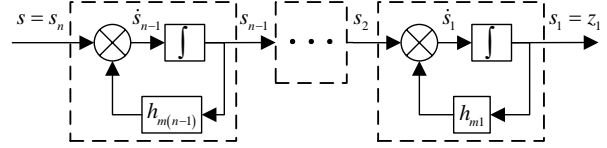


Figure 11: Fully actuated iterative manifold diagram.

differential explosion may occur due to the iterative generation of the manifold. This may require finding a non-linear fast manifold construction method that does not rely on iteration.

A Proof of Lemma 1

The fully actuated iterative manifold can be rewritten as:

$$s = \prod_{i=1}^{n-1} \left(\frac{\partial}{\partial t} - \frac{h_{mi}}{s_i} \right) s_1 \quad (69)$$

According the definition of h_{mi} in (11) and **Assumption 6**, there must exist positive constants $r_i, i = 1, \dots, n-1$ such that $s = 0$ has $n-1$ negative real roots $\frac{h_{mi}}{s_i} < -r_i$, and there is a positive constant \bar{s} such that $|s| < \bar{s}$ since \mathbf{Z} can be maintained at the vicinity of the manifold $s = 0$ when $|\xi(\mathbf{Z})| < 1$.

The iterative manifold can be considered as a series of first order linear low pass filters as shown in Fig. 11. Referring to the Proposition 2 in [32], it can be obtained that there exist positive constants \bar{s}_i and \bar{z}_i such that

$$|s_i| \leq \bar{s}_i + \frac{\bar{s}}{\prod_{j=i}^{n-1} r_j} \quad (70)$$

and

$$|z_i| \leq \bar{z}_i + \frac{2^{n-1-i} \bar{s}}{\prod_{j=i}^{n-1} r_j} \quad (71)$$

for all $t \geq 0, i = 1, \dots, n-1$.

B Proof of Theorem 1

From Assumptions 4-6 and the design of the x_U, x_L, y_U, y_L in (21) and (22), it can be obtained that $\mathbf{Z}(0) \in \Psi_s, \xi(0) \in (-1, 1)$, and all signals are bounded at the beginning.

We can prove the theorem in two different situations as following: situation A is $\frac{\partial h_{m(n-1)}(\bullet)}{\partial \bullet} \in L_\infty$, and situation B is $\lim_{\bullet \rightarrow 0} \frac{\partial h_{m(n-1)}(\bullet)}{\partial \bullet} = -\infty$.

Proof for situation A ($\frac{\partial h_{m(n-1)}(\bullet)}{\partial \bullet} \in L_\infty$):

By seeking a contradiction, it is to be proved that and

$$|\xi| < 1, \forall t \geq 0 \quad (72)$$

so that $\mathbf{Z}(t) \in \Psi_s$ according to the definition of ξ in (28).

Since the variables in the manifold constraint variable system (80) are all continuous. According to the intermediate value theorem for continuous functions, if the system violates the manifold constraint, i.e. exists $|\xi(t_v)| \geq 1$, then there must exists a moment $t_c \in (0, t_v]$, which denotes the time instant when (72) is violated for the first time, that

$$\lim_{t \rightarrow t_c^-} |\xi| = 1 \quad (73)$$

and

$$\lim_{t \rightarrow t_c^-} \frac{\partial |\xi|}{\partial t} = \lim_{|\xi| \rightarrow 1^-} \frac{\partial |\xi|}{\partial t} \geq 0. \quad (74)$$

It can guarantee that $\xi \in (-1, 1)$ and all signals are bounded for $t \in [0, t_c)$ from **Lemma 1**. The following discussions from (75) to (84) are based on the time interval $[0, t_c)$.

According to (28), the manifold constraint variable system can be expressed as:

$$\dot{\xi} = 2.$$

$$\begin{cases} \frac{\dot{s}_{n-1} - \dot{x}_c - \dot{x}_L}{x_U - x_L} + \frac{(s_{n-1} - x_c - x_L)(\dot{x}_U - \dot{x}_L)}{(x_U - x_L)^2} \\ \quad , \text{ OMC} \\ \frac{\dot{s} - \dot{y}_L}{y_U - y_L} + \frac{(s - y_L)(\dot{y}_U - \dot{y}_L)}{(y_U - y_L)^2} \\ \quad , \text{ LoMC} \\ \frac{\dot{s}_{n-1} - h'_v \ddot{s}_{n-1} - \dot{x}_L}{x_U - x_L} + \frac{(s_{n-1} - h_v - x_L)(\dot{x}_U - \dot{x}_L)}{(x_U - x_L)^2} \\ \quad , \text{ LaMC} \end{cases} \dot{\xi} = 2.$$

$$= 2 \cdot \begin{cases} \frac{-\dot{x}_c}{x_U - x_L} + C_1, & \text{ OMC} \\ \frac{\dot{s}}{y_U - y_L} + C_2, & \text{ LoMC} \\ \frac{-h'_v \ddot{s}_{n-1}}{x_U - x_L} + C_3, & \text{ LaMC} \end{cases} \quad (75)$$

where $C_1 = \frac{\dot{s}_{n-1} - \dot{x}_L}{x_U - x_L} + \frac{(s_{n-1} - x_c - x_L)(\dot{x}_U - \dot{x}_L)}{(x_U - x_L)^2}$, $C_2 = \frac{-\dot{y}_L}{y_U - y_L} + \frac{(s - y_L)(\dot{y}_U - \dot{y}_L)}{(y_U - y_L)^2}$, and $C_3 = \frac{\dot{s}_{n-1} - \dot{x}_L}{x_U - x_L} + \frac{(s_{n-1} - h_v - x_L)(\dot{x}_U - \dot{x}_L)}{(x_U - x_L)^2}$ are all bounded.

According to (11) and (12), it can be obtained that

$$\dot{s}_{n-1} = s + h_{m(n-1)}(s_{n-1}) = z_n - \sum_{i=1}^{n-2} h_{mi}^{(n-1-i)}(s_i) \quad (76)$$

$$\ddot{s}_{n-1} = \dot{z}_n - \sum_{i=1}^{n-2} h_{mi}^{(n-i)}(s_i) \quad (77)$$

Simultaneously taking the derivative of both sides of equation (27) yields

$$\begin{aligned} \frac{\partial h_{m(n-1)}(x_c)}{\partial x_c} \dot{x}_c &= \frac{\dot{y}_U x_U - y_U \dot{x}_U}{x_U^2} (x_c - s_{n-1}) \\ &+ \frac{y_U}{x_U} (\dot{x}_c - \dot{s}_{n-1}) + \ddot{s}_{n-1} \end{aligned} \quad (78)$$

Therefore, it can be obtained that

$$\begin{aligned} \dot{x}_c &= \frac{\frac{\dot{y}_U x_U - y_U \dot{x}_U}{x_U^2} (x_c - s_{n-1}) - \frac{y_U}{x_U} \dot{s}_{n-1} + \ddot{s}_{n-1}}{\frac{\partial h_{m(n-1)}(x_c)}{\partial x_c} - \frac{y_U}{x_U}} \\ &= A_1 \ddot{s}_{n-1} + B_1 = A_1 \dot{z}_n - A_1 \sum_{i=1}^{n-2} h_{mi}^{(n-i)}(s_i) + B_1 \end{aligned} \quad (79)$$

in which $A_1 = \frac{1}{\frac{\partial h_{m(n-1)}(x_c)}{\partial x_c} - \frac{y_U}{x_U}}$ and $B_1 = \frac{\frac{\dot{y}_U x_U - y_U \dot{x}_U}{x_U^2} (x_c - s_{n-1}) - \frac{y_U}{x_U} \dot{s}_{n-1}}{\frac{\partial h_{m(n-1)}(x_c)}{\partial x_c} - \frac{y_U}{x_U}}$ are both bounded and $-A_1$ has a positive lower bound since $\frac{\partial h_{m(n-1)}(x_c)}{\partial x_c} < 0$.

By substituting (77), (79), and the controller (29), the manifold constraint variable system (75) can be rewritten as:

$$\begin{cases} -\frac{A_1 \dot{z}_n - A_1 \sum_{i=1}^{n-2} h_{mi}^{(n-i)}(s_i) + B_1}{x_U - x_L} + C_1, & \text{ OMC} \\ \frac{\dot{z}_n - \sum_{i=1}^{n-1} h_{mi}^{(n-i)}(s_i)}{y_U - y_L} + C_2, & \text{ LoMC} \\ \frac{-h'_v (\dot{z}_n - \sum_{i=1}^{n-2} h_{mi}^{(n-i)}(s_i))}{x_U - x_L} + C_3, & \text{ LaMC} \end{cases} \dot{\xi} = 2.$$

$$= A \dot{z}_n + D = -AGk_u \Gamma(\xi) + AF + D \quad (80)$$

where $h'_v := \frac{\partial h_v(\dot{s}_{n-1})}{\partial \dot{s}_{n-1}}$ and

$$A = 2 \cdot \begin{cases} -\frac{A_1}{x_U - x_L}, & \text{ OMC} \\ \frac{1}{y_U - y_L}, & \text{ LoMC} \\ \frac{-h'_v}{x_U - x_L}, & \text{ LaMC} \end{cases} \quad (81)$$

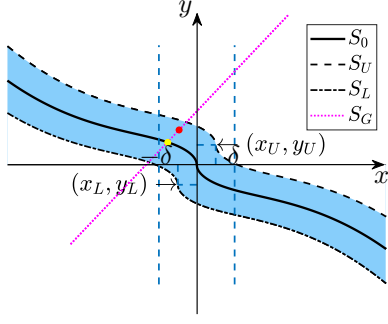


Figure 12: Manifold constraint diagram under situation B.

$$D = 2 \cdot \begin{cases} -\frac{-A_1 \sum_{i=1}^{n-2} h_{mi}^{(n-i)}(s_i) + B_1}{x_U - x_L} + C_1, & \text{OMC} \\ -\frac{\sum_{i=1}^{n-1} h_{mi}^{(n-i)}(s_i)}{y_U - y_L} + C_2, & \text{LoMC} \\ \frac{h'_v \sum_{i=1}^{n-2} h_{mi}^{(n-i)}(s_i)}{x_U - x_L} + C_3, & \text{LaMC} \end{cases} \quad (82)$$

Since $\frac{\partial h_{m(n-1)}(\bullet)}{\partial \bullet} < 0$ and $\frac{\partial h_{m(n-1)}(\bullet)}{\partial \bullet} \in L_\infty$, the value $-h'_v$ is bounded with a positive lower bound. There exist positive constants \underline{A} , \bar{A} , \bar{D} , and \bar{F} such that $0 < \underline{A} \leq A \leq \bar{A}$, $|D| \leq \bar{D}$, and $|F| \leq \bar{F}$.

It holds that

$$\frac{\partial |\xi|}{\partial t} \leq -\underline{A} \underline{G} k_u |\Gamma(\xi)| + \bar{A} \bar{F} + \bar{D} < 0 \quad (83)$$

when $|\xi| > \Gamma^{-1}(\frac{\bar{A}\bar{F} + \bar{D}}{\underline{A}\underline{G}k_u})$, and

$$\lim_{|\xi| \rightarrow 1^-} \frac{\partial |\xi|}{\partial t} = \lim_{|\Gamma(\xi)| \rightarrow \infty} \frac{\partial |\xi|}{\partial t} = -\infty. \quad (84)$$

This contradicts with (74), therefore the assumption is not valid, $|\xi| < 1$ for all time and the constraint is satisfied in situation A.

Proof for situation B ($\lim_{\bullet \rightarrow 0} \frac{\partial h_{m(n-1)}(\bullet)}{\partial \bullet} = -\infty$):

For situation B, there exists a positive value δ that satisfies

$$h_{m(n-1)}(\delta - x_U) = -y_U. \quad (85)$$

$\frac{\partial h_{m(n-1)}(s_{n-1})}{\partial s_{n-1}} \in L_\infty$ for $s_{n-1} \notin \Omega_\delta \triangleq (-\delta, \delta)$. System fully actuated errors \mathbf{Z} maintains in Ψ_s when $s_{n-1} \notin \Omega_\delta$ as the proof for situation A.

According to $\mathbf{Z}(0) \in \Psi_s$ and the proof for situation A, there exists $t_\delta \geq 0$ so that $\mathbf{Z} \in \Psi_s$ and $s_{n-1} \in \Omega_\delta$. The red bullet in Fig. 12 is the position $(s_{n-1}(t), \dot{s}_{n-1}(t))$ with $t \geq t_\delta$. The yellow bullet in Fig. 12 is the position $(x_c(t), y_c(t))$. Additionally, there exists a positive constant \bar{s}_{n-1} so that

$|\dot{s}_{n-1}| \leq \bar{s}_{n-1}$ for $\mathbf{Z} \in \Psi_s$ and $s_{n-1} \in \Omega_\delta$, and the horizontal distance δ_x between the red bullet and the boundary S_U or S_L under $s_{n-1} \in \Omega_\delta$ satisfies that $0 < \delta_x(t_\delta) < 2\delta$. There exists a positive constant $t_{mx} = 2\delta(t_\delta)/\bar{s}_{n-1}$ that the time for the red bullet to move to the boundary t_{mx} satisfies that $t_{mx} > t_{my}$. The time for the red bullet to move to the horizontal axis $\dot{s}_{n-1} = 0$ is t_{my} .

According to (77),

$$\int_{\dot{s}_{n-1}(t_\delta)}^0 \frac{d\dot{s}_{n-1}}{\ddot{s}_{n-1}} = \int_{t_\delta}^{t_\delta + t_{my}} dt \quad (86)$$

and

$$\begin{aligned} t_{my} &= \int_{\dot{s}_{n-1}(t_\delta)}^0 \frac{1}{\dot{z}_n - A_M} d\dot{s}_{n-1} \\ &= \int_{\dot{s}_{n-1}(t_\delta)}^0 \frac{1}{-Gk_u \Gamma(\xi) + F - A_M} d\dot{s}_{n-1} \end{aligned} \quad (87)$$

where $A_M = \sum_{i=1}^{n-2} h_{mi}^{(n-i)}(s_i)$ and it has an upper bound \bar{A}_M according to the properties of h_{mi} . Therefore, in the worst-case scenario, the red bullet moves close to the boundary, $t_{my} < t_{mx}$ as long as $\Gamma^{-1}(\frac{\bar{s}_{n-1}^2/(2\delta(t_\delta)) + \bar{F}_d + \bar{A}_M}{\underline{G}k_u}) \leq |\xi| < 1$, that is, the red bullet always can cross the horizontal axis $\dot{s}_{n-1} = 0$ before touching the boundary. Then the red bullet will move in the opposite direction, making it impossible to cross the boundary.

Furthermore, since all signals are bounded for $t \geq 0$, there exists a positive constant $\bar{\xi}$ such that $|\xi| \leq \bar{\xi} < 1$, which implies that the controller has an upper bound $\tilde{u} = k_u \Gamma(\bar{\xi})$.

C Proof of Theorem 2

According to the designs in (30), when the distance between the current state $(s_{n-1}(t), ds_{n-1}(t)) \in \Psi_s$ and the boundaries $\mathbf{S}_U, \mathbf{S}_L$ greater than ρ_e , the flexible constraint boundaries in (30) equals the original constraint boundaries in (21) and (22), and the flexible constraint variable $\tilde{\xi}$ in (31) equals the original constraint variable ξ in (28), making the flexible controller in (32) identical to the controller in (29).

When the distance between the current state $(s_{n-1}(t), ds_{n-1}(t))$ and the manifold constraint boundaries \mathbf{S}_U and \mathbf{S}_L is less than ρ_e , the flexible constraint boundaries $\tilde{x}_U, \tilde{x}_L, \tilde{y}_U, \tilde{y}_L$ in (30) expand based on the original constraint boundary x_U, x_L, y_U, y_L in (21) and (22). After the current state exceeds the original manifold constraint boundaries \mathbf{S}_U and \mathbf{S}_L , $\mathcal{T}_s = 1$ in (30) can be obtained, the flexible expanded constraint (30) ensures that the

distance between the current state and the flexible boundaries remains ρ_e , so the absolute value of the flexible constraint variable $\tilde{\xi}$ can be redefined as

$$|\tilde{\xi}| = \frac{d_{sc}}{d_{sc} + \rho_e} < 1. \quad (88)$$

This guarantees that the flexible controller is well-defined and ensures the effective operation of the controller. If the system is not ISS and ISpS, as d_{sc} increases, $|\tilde{\xi}|$ continues to increase and approaches 1, while the flexible controller also continues to increase and tends to infinity.

Based on the above analysis, there must exist a sufficiently small positive constant $\bar{\rho}_e$

$$\bar{\rho}_e = \min \left\{ d_U - \Gamma^{-1} \left(\frac{\max\{\bar{u}, -u\}}{k_u} \right) \right\}, \quad (89)$$

such that the controller will enter saturation before flexible expansion is activated for $\rho_e \in (0, \bar{\rho}_e]$. In this case, if the actuator output capability is sufficient, the controller will not reach the input constraint (6), thus achieving the same control effect as in Theorem 1 (i) and (ii). If the actuator output capability is insufficient, as the state approaches the constraint boundary, the system will first enter saturation, and then proceed with the flexible expansion of the constraint boundary as (30). In the reverse process, as the state $(s_{n-1}(t), ds_{n-1}(t))$ moves back from outside the original constraint set Ψ_s to within the set as $(s_{n-1}(t), ds_{n-1}(t)) \in \Psi_s$, when the distance to the constraint boundary exceeds ρ_e , the flexible constraint boundary will restore to the original constraint value, i.e., $\tilde{x}_U = -\tilde{x}_L = x_U = -x_L$ and $\tilde{y}_U = -\tilde{y}_L = y_U = -y_L$, since $\mathcal{T}_s = 0$ in (30). This ensures that when the controller exits saturation, the flexible constraint boundary has been fully restored to the original constraint.

D Proof of Theorem 3

Define the scaled estimation errors as:

$$\zeta_i = \frac{z_i - \hat{z}_i}{\mu^{n-i}}, \quad i = 1, \dots, n \quad (90)$$

Therefore, $\hat{\mathbf{Z}} = \mathbf{Z} - \mathcal{D}(\mu)\zeta$ with $\mathcal{D}(\mu) = \text{diag}(\mu^{n-1}, \dots, \mu, 1)$ and $\zeta = [\zeta_1, \dots, \zeta_n]^T$.

The derivative of ζ is

$$\dot{\zeta} = \frac{1}{\mu}(\mathbf{A} - \mathbf{H}\mathbf{C})\zeta + \mathcal{B}(Gu + F) \quad (91)$$

with $H = [a_1, a_2, \dots, a_n]^T$.

From Assumptions 4-6, there exist positive constants $\bar{\xi} < 1$, $\bar{\mathbf{Z}}$, and τ_2 that $(\xi, \mathbf{Z}) \in \Psi_{\xi Z}, \forall t \in [0, \tau_2]$, where $\Psi_{\xi Z}$ is a set defined as $\Psi_{\xi Z} = \{(\xi, \mathbf{Z}) \mid |\xi| \leq \bar{\xi}, \|\mathbf{Z}\| \leq \bar{\mathbf{Z}}\}$. Hence, it can be found positive constant $\bar{\Delta}$ that $Gu + F \leq \bar{\Delta}, \forall t \in [0, \tau_2]$.

Define Lyapunov function $V_\zeta = \zeta^T \mathcal{P} \zeta$ where positive definite symmetric matrix $\mathcal{P} \in \mathcal{R}^{n \times n}$ is the solution of $\mathcal{P}(\mathbf{A} - \mathbf{H}\mathbf{C}) + (\mathbf{A} - \mathbf{H}\mathbf{C})^T \mathcal{P} = -\mathbf{I}_n$. Differentiating V_ζ with respect to time yields

$$\begin{aligned} \dot{V}_\zeta &= -\frac{1}{\mu} \zeta^T \zeta + 2\zeta^T \mathcal{P} \mathcal{B}(Gu + F) \\ &\leq -\frac{1}{\mu} \|\zeta\|^2 + 2\|\zeta\| \|\mathcal{P}\| \bar{\Delta} \\ &\leq -\frac{1}{\mu} \|\zeta\|^2 + \frac{1}{2\mu} \|\zeta\|^2 + 2\mu \|\mathcal{P}\|^2 \bar{\Delta}^2 \\ &\leq -\frac{1}{2\mu \|\mathcal{P}\|} V_\zeta + 2\mu \|\mathcal{P}\|^2 \bar{\Delta}^2. \end{aligned} \quad (92)$$

Since the convergence rate of V_ζ will be faster and faster as well as the convergence error will be smaller and smaller when μ tends to 0, there must be a small positive constant μ_1 and $\tau_1 < \tau_2$ to make $\|\zeta\| \leq \bar{\zeta}$ when $\mu \in (0, \mu_1)$ and $t \in (\tau_1, \tau_2]$ for any positive constant $\bar{\zeta}$.

Considering that the controller structure is Lipschitz, there must exist positive constants \mathcal{L} and $\mu_2 < 1$ for any $\mu \in (0, \mu_2)$ such that

$$\|v(\hat{\mathbf{Z}}) - v(\mathbf{Z})\| = \|v(\mathbf{Z} - \mathcal{D}(\mu)\zeta) - v(\mathbf{Z})\| \leq \mathcal{L} \|\zeta\|. \quad (93)$$

Therefore there exists a positive constant μ_3 such that for $\mu \in (0, \mu_3)$, $\|\zeta\|$, $\|\hat{\mathbf{Z}} - \mathbf{Z}\|$, and \mathcal{L} are all sufficiently small, hence **Theorem 2** can be used to obtain the same conclusion since the error of the v is bounded. Thus $\mathbf{Z}(t) \in \Psi_s$ holds for $t \geq 0$ when $0 < \mu < \min(\mu_1, \mu_2, \mu_3) = \bar{\mu}$.

References

References

- [1] D. Swaroop, J. K. Hedrick, P. P. Yip, and J. C. Gerdes, "Dynamic surface control for a class of nonlinear systems," *IEEE transactions on automatic control*, vol. 45, no. 10, pp. 1893–1899, 2000.
- [2] J.-X. Zhang and G.-H. Yang, "Fuzzy adaptive output feedback control of uncertain nonlinear systems with prescribed performance," *IEEE transactions on cybernetics*, vol. 48, no. 5, pp. 1342–1354, 2017.

- [3] S. Zhou, Y. Song, and C. Wen, “Event-triggered practical prescribed time output feedback neuroadaptive tracking control under saturated actuation,” *IEEE Transactions on Neural Networks and Learning Systems*, vol. 34, no. 8, pp. 4717–4727, 2021.
- [4] G. Liu, J. H. Park, H. Xu, and C. Hua, “Reduced-order observer-based output-feedback tracking control for nonlinear time-delay systems with global prescribed performance,” *IEEE Transactions on Cybernetics*, vol. 53, no. 9, pp. 5560–5571, 2022.
- [5] Y. Li, S. Ma, K. Li, and S. Tong, “Adaptive fuzzy output feedback fault-tolerant control for active suspension systems,” *IEEE Transactions on Intelligent Vehicles*, vol. 9, no. 1, pp. 2469–2478, 2023.
- [6] X. Zhang and W. Lin, “A k-filter-based adaptive control for nonlinear systems with unknown parameters in state and output equations,” *Automatica*, vol. 105, pp. 186–197, 2019.
- [7] Y. Wang and Y. Liu, “Global practical tracking via adaptive output feedback for uncertain nonlinear systems without polynomial constraint,” *IEEE Transactions on Automatic Control*, vol. 66, no. 4, pp. 1848–1855, 2020.
- [8] I. Kanellakopoulos, P. V. Kokotovic, and A. S. Morse, “Systematic design of adaptive controllers for feedback linearizable systems,” in *1991 American control conference*. IEEE, 1991, pp. 649–654.
- [9] G. Duan, “High-order fully actuated system approaches: Part ii. generalized strict-feedback systems,” *International Journal of Systems Science*, vol. 52, no. 3, pp. 437–454, 2021.
- [10] M. Cai, X. He, and D. Zhou, “An active fault tolerance framework for uncertain nonlinear high-order fully-actuated systems,” *Automatica*, vol. 152, p. 110969, 2023.
- [11] I. S. Dimanidis, C. P. Bechlioulis, and G. A. Rovithakis, “Output feedback approximation-free prescribed performance tracking control for uncertain mimo nonlinear systems,” *IEEE Transactions on Automatic Control*, vol. 65, no. 12, pp. 5058–5069, 2020.
- [12] V. Utkin, “Variable structure systems with sliding modes,” *IEEE Transactions on Automatic control*, vol. 22, no. 2, pp. 212–222, 1977.
- [13] J.-J. E. Slotine and W. Li, “On the adaptive control of robot manipulators,” *The international journal of robotics research*, vol. 6, no. 3, pp. 49–59, 1987.
- [14] J. Han, “From pid to active disturbance rejection control,” *IEEE transactions on Industrial Electronics*, vol. 56, no. 3, pp. 900–906, 2009.
- [15] C. P. Bechlioulis and G. A. Rovithakis, “A low-complexity global approximation-free control scheme with prescribed performance for unknown pure feedback systems,” *Automatica*, vol. 50, no. 4, pp. 1217–1226, 2014.
- [16] Y. Cao, Z. Shen, J. Cao, D. Li, and Y. Song, “Prescribed time recovery from state constraint violation via approximation-free control approach,” *IEEE Transactions on Circuits and Systems I: Regular Papers*, 2023.
- [17] W. M. Haddad, J. Lee, and S. P. Bhat, “Asymptotic and finite-time semistability for nonlinear discrete-time systems with application to network consensus,” *IEEE Transactions on Automatic Control*, vol. 68, no. 2, pp. 766–781, 2022.
- [18] C.-C. Hua, Q.-D. Li, and K. Li, “Event-based finite-time control for high-order interconnected nonlinear systems with asymmetric output constraints,” *IEEE Transactions on Automatic Control*, vol. 67, no. 11, pp. 6135–6142, 2021.
- [19] H. Min, S. Xu, B. Zhang, and N. Duan, “Practically finite-time control for nonlinear systems with mismatching conditions and application to a robot system,” *IEEE Transactions on Systems, Man, and Cybernetics: Systems*, vol. 50, no. 2, pp. 480–489, 2017.
- [20] W. Mi, L. Luo, and S. Zhong, “Fixed-time consensus tracking for multi-agent systems with a nonholonomic dynamics,” *IEEE Transactions on Automatic Control*, vol. 68, no. 2, pp. 1161–1168, 2022.
- [21] C. Hua, Y. Li, and X. Guan, “Finite/fixed-time stabilization for nonlinear interconnected systems with dead-zone input,” *IEEE Transactions on Automatic Control*, vol. 62, no. 5, pp. 2554–2560, 2016.
- [22] Y. Zhou, J. Zhou, S. Wang, and G. Wen, “Practical fixed-time attitude consensus tracking for multi-quadrotor systems: A composite learning backstepping approach,” *IEEE Transactions on Circuits and Systems II: Express Briefs*, 2024.

- [23] A. J. Munoz-Vazquez, J. D. Sánchez-Torres, E. Jimenez-Rodriguez, and A. G. Loukianov, “Predefined-time robust stabilization of robotic manipulators,” *IEEE/ASME Transactions on Mechatronics*, vol. 24, no. 3, pp. 1033–1040, 2019.
- [24] A. Ilchmann, E. P. Ryan, and C. J. Sangwin, “Tracking with prescribed transient behaviour,” *ESAIM: Control, Optimisation and Calculus of Variations*, vol. 7, pp. 471–493, 2002.
- [25] C. P. Bechlioulis and G. A. Rovithakis, “Robust adaptive control of feedback linearizable mimo nonlinear systems with prescribed performance,” *IEEE Transactions on Automatic Control*, vol. 53, no. 9, pp. 2090–2099, 2008.
- [26] A. Shakouri and N. Assadian, “Prescribed-time control for perturbed euler-lagrange systems with obstacle avoidance,” *IEEE Transactions on Automatic Control*, vol. 67, no. 7, pp. 3754–3761, 2021.
- [27] C. Hua, P. Ning, and K. Li, “Adaptive prescribed-time control for a class of uncertain nonlinear systems,” *IEEE Transactions on Automatic Control*, vol. 67, no. 11, pp. 6159–6166, 2021.
- [28] Y. Cao, J. Cao, and Y. Song, “Practical prescribed time tracking control over infinite time interval involving mismatched uncertainties and non-vanishing disturbances,” *Automatica*, vol. 136, p. 110050, 2022.
- [29] J. Ni, L. Liu, C. Liu, and J. Liu, “Fixed-time leader-following consensus for second-order multiagent systems with input delay,” *IEEE Transactions on Industrial Electronics*, vol. 64, no. 11, pp. 8635–8646, 2017.
- [30] Z. Chen, X. Ju, Z. Wang, and Q. Li, “The prescribed time sliding mode control for attitude tracking of spacecraft,” *Asian Journal of Control*, vol. 24, no. 4, pp. 1650–1662, 2022.
- [31] L. Zhang, L. Zhu, and C. Hua, “Practical prescribed time control based on high-order fully actuated system approach for strong interconnected nonlinear systems,” *Nonlinear Dynamics*, vol. 110, no. 4, pp. 3535–3545, 2022.
- [32] C. P. Bechlioulis, A. Theodorakopoulos, and G. A. Rovithakis, “Output feedback stabilization with prescribed performance for uncertain nonlinear systems in canonical form,” in *52nd IEEE Conference on Decision and Control*. IEEE, 2013, pp. 5084–5089.
- [33] C. Wei, J. Luo, Z. Yin, X. Wei, and J. Yuan, “Robust estimation-free decentralized prescribed performance control of nonaffine nonlinear large-scale systems,” *International Journal of Robust and Nonlinear Control*, vol. 28, no. 1, pp. 174–196, 2018.
- [34] M. Lv and N. Wang, “Distributed control for uncertain multi-agent systems with the powers of positive-odd numbers: A low-complexity design approach,” *IEEE Transactions on Automatic Control*, 2023.
- [35] Y. Song, Y. Wang, and C. Wen, “Adaptive fault-tolerant pi tracking control with guaranteed transient and steady-state performance,” *IEEE Transactions on automatic control*, vol. 62, no. 1, pp. 481–487, 2016.
- [36] Y. Cao and Y.-D. Song, “Adaptive pid-like fault-tolerant control for robot manipulators with given performance specifications,” *International Journal of Control*, vol. 93, no. 3, pp. 377–386, 2020.
- [37] P. S. Trakas and C. P. Bechlioulis, “Adaptive performance control for input constrained mimo nonlinear systems,” *IEEE Transactions on Systems, Man, and Cybernetics: Systems*, 2024.
- [38] T. Berger, “Input-constrained funnel control of nonlinear systems,” *IEEE Transactions on Automatic Control*, 2024.
- [39] Y. Su, “Comments on “fixed-time sliding mode control with mismatched disturbances”[*automatica* 136 (2022) 110009],” *Automatica*, vol. 151, p. 110916, 2023.
- [40] E. Moulay, V. Léchappé, E. Bernuau, and F. Plestan, “Robust fixed-time stability: Application to sliding-mode control,” *IEEE Transactions on Automatic Control*, vol. 67, no. 2, pp. 1061–1066, 2021.
- [41] E. Moulay, V. Léchappé, E. Bernuau, M. Defoort, and F. Plestan, “Fixed-time sliding mode control with mismatched disturbances,” *Automatica*, vol. 136, p. 110009, 2022.
- [42] F. Fotiadis and G. A. Rovithakis, “Input-constrained prescribed performance control for high-order mimo uncertain nonlinear systems via reference modification,” *IEEE Transactions on Automatic Control*, vol. 69, no. 5, pp. 3301–3308, 2023.

- [43] Y. Wu, X. Yu, and Z. Man, “Terminal sliding mode control design for uncertain dynamic systems,” *Systems & Control Letters*, vol. 34, no. 5, pp. 281–287, 1998.
- [44] J. Yang, X. Yu, L. Zhang, and S. Li, “A lyapunov-based approach for recursive continuous higher order nonsingular terminal sliding-mode control,” *IEEE Transactions on Automatic Control*, vol. 66, no. 9, pp. 4424–4431, 2020.
- [45] H. Zhang, B. Li, B. Xiao, Y. Yang, and J. Ling, “Nonsingular recursive-structure sliding mode control for high-order nonlinear systems and an application in a wheeled mobile robot,” *ISA transactions*, vol. 130, pp. 553–564, 2022.